

# Zero-temperature Kosterlitz-Thouless transition in a two-dimensional quantum system

Claudio Castelnovo <sup>a, 1</sup> Claudio Chamon <sup>a, 1</sup> Christopher Mudry <sup>b</sup>  
Pierre Pujol <sup>c</sup>

<sup>a</sup>*Physics Department, Boston University, Boston, MA 02215, USA*

<sup>b</sup>*Condensed Matter Theory Group, Paul Scherrer Institut, CH-5232 Villigen PSI,  
Switzerland*

<sup>c</sup>*Laboratoire de Physique, École Normale Supérieure, 46 Allée d'Italie, 69364 Lyon  
Cedex 07, France*

---

## Abstract

We construct a local interacting quantum dimer model on the square lattice, whose zero-temperature phase diagram is characterized by a line of critical points separating two ordered phases of the valence bond crystal type. On one side, the line of critical points terminates in a quantum transition inherited from a Kosterlitz-Thouless transition in an associated classical model. We also discuss the effect of a longer-range dimer interaction that can be used to suppress the line of critical points by gradually shrinking it to a single point. Finally, we propose a way to generalize the quantum Hamiltonian to a dilute dimer model in presence of monomers and we qualitatively discuss the phase diagram.

*Key words:* quantum dimer model, quantum criticality, Kosterlitz-Thouless transition, conformal field theory, Stochastic Matrix Form decomposition

*PACS:* 75.30.Kz, 75.40.Mg, 74.20.Mn, 11.25.Hf

---

## 1 Introduction

Dimer models are of interest to a variety of scientific disciplines from chemistry to mathematics and physics. In chemistry, dimers are used, for example, to model

---

Corresponding author.

*Email addresses:* castel@buphy.bu.edu (Claudio Castelnovo),  
chamon@buphy.bu.edu (Claudio Chamon), christopher.mudry@psi.ch  
(Christopher Mudry), pierre.pujol@ens-lyon.fr (Pierre Pujol).

<sup>1</sup> This work is supported in part by the NSF Grants DMR-0305482 and DMR-0403997.

molecules deposited on crystalline surfaces and to study their thermodynamic properties [1]. In mathematics, dimers are often used to construct combinatorial and folding problems such as the domino tiling of a two-dimensional (2D) plane [2]. In physics, dimer models have been elevated from problems in classical statistical physics [3, 4, 5, 6, 7, 8, 9, 10], to problems in quantum statistical physics [11, 12, 13, 14, 15, 16, 17, 18, 19, 20, 21, 22, 23, 24, 25, 26, 27, 28, 29, 30, 31, 32, 33, 34, 35, 36, 37, 38, 39], with the advent of high- $T_c$  superconductivity. In particular, quantum dimer models can provide examples of strongly correlated quantum systems for which the zero temperature phase diagram is characterized by exotic quantum phase transitions that fall out of the classification of phase transitions proposed by Landau [40, 41]. Furthermore, the finite-temperature phase diagram of quantum dimer models might give some insight into the phenomenological observation that scaling laws extend to surprisingly high temperatures in some strongly correlated systems [42, 43].

In this paper, we show how dimer models can be used as a laboratory to construct quantum Hamiltonians displaying phase transitions that cannot be understood in terms of a local order parameter, i.e., phase transitions that cannot be encoded by an effective theory of the Landau-Ginzburg type, a topic of renewed interest in condensed matter physics [40, 41]. Perhaps the most famous counter example to a phase transition described with a Landau-Ginzburg action for a local order parameter is the Kosterlitz-Thouless (KT) transition. The KT transition is a weak essential singularity of the free energy for a phase-like order parameter with support in 2D Euclidean space. It is interpreted as the unbinding of topological defects (vortices) in the order parameter. The main result of this paper is the construction of a quantum dimer model with *local interactions* on the square lattice [Eqs. (13,14)] that undergoes a quantum phase transition of the KT type when measured by the spatial decay of equal-time correlation functions.

It is well known that quantum phase transitions can be of the KT type in 1D systems with dynamical exponent  $z = 1$  relating the scaling in space to the scaling in time. For example, a 1D Luttinger liquid can be unstable to a charge-ordered density wave through a KT transition. This is so because the quantum field theory describing the quantum phase transition for interacting fermions is related through bosonization to a scalar field theory, the Sine-Gordon model. Analytical continuation of time to imaginary time can be used to turn (Minkowski) space-time into 2D Euclidean space while the Poincaré symmetry group becomes symmetry under translations and rotations. Evidently, if a quantum phase transition can be described by a local quantum field theory in  $D + 1$  space-time that turns into a local classical action undergoing a classical phase transition in  $D + 1$  Euclidean space upon analytical continuation of time to imaginary time [44], then this quantum phase transition cannot be associated to a KT transition when  $z = 1$  and  $D \geq 2$ . Viewed against this no-go theorem, it is remarkable that some equal-time correlation functions of a 2D quantum dimer model with local interactions and defined on the square lattice [Eqs. (13,14)] share the hallmarks of a KT transition.

Since the quantum Hamiltonian of our 2D lattice model, defined in Eqs. (13) and (14), has only local interactions, it is safe to argue that unequal-time correlations should show algebraic behavior if the equal-time correlations do so. The reason is that a local Hamiltonian with algebraic spatial correlations should be gapless. A rigorous proof of this statement was given by Hastings in Ref. [45]. The converse statement is known not to be true, as shown in Ref. [46]. A local quantum Hamiltonian may be gapless but have only short-ranged spatial correlations between local operators. Therefore, while in this paper we concentrate solely on equal-time correlation functions, the KT-like transition identified through the algebraic spatial correlations should be manifest in unequal-time correlation functions related to the spatial ones through a dynamical exponent  $z$ . Moreover, a dynamical exponent  $z = 2$  is suggested by our mapping of the quantum system onto a classical model with local stochastic dynamics [16, 28, 33].

What is the continuum imaginary-time field theory that captures the low-energy physics of the local quantum lattice Hamiltonian, Eqs. (13,14), when fine-tuned to its line of critical points? We expect it to be that of a classical Lifshitz point problem in a uniform magnetic field introduced by Grinstein in Ref. [47]. Here, a short-ranged anisotropic coupling between 2D layers, each of which are described by a local classical Lagrangian, is interpreted as the coupling between imaginary-time slices of the quantum problem [29, 48]. Note, however, that it is not always the case that a *local* classical Lagrangian in  $D + 1$  Euclidean space corresponds to a *local* quantum Hamiltonian in  $D$  spatial dimensions; a counter-example was shown in Ref. [49]. Our 2D lattice realization of the quantum KT-transition starts directly from the local quantum Hamiltonian, and avoids any discussion of the corresponding classical imaginary-time Lagrangian.

The quantum dimer model on the square lattice discussed in the present paper, Eqs. (13,14), is represented by a symmetric and positive matrix that obeys the so-called Stochastic Matrix Form (SMF) decomposition [28, 29, 33]. The advantages of an SMF decomposition of a quantum Hamiltonian are three-fold. First, at least one ground state (GS) can be obtained exactly in terms of the parameters entering the SMF quantum Hamiltonian, see Eq. (16) [12, 16, 28, 29, 33]. Second, one can construct a classical configuration space that is in one-to-one correspondence with the orthonormal basis in which the SMF quantum Hamiltonian is represented. On this configuration space, a classical partition function can be uniquely defined from the GS wavefunction, see Eq. (19) [12, 16, 28, 29, 33], such that zero-temperature and equal-time correlation functions of quantum operators diagonal in the SMF basis are equivalent to equilibrium thermal averages of corresponding quantities in the classical system. Note that the possibility to use classical numerical techniques, such as Monte Carlo simulations and transfer matrix calculations, in the *same number of dimensions* gives access to much larger system sizes than quantum techniques, such as quantum Monte Carlo or exact diagonalization routines, do. Third, the parameters entering the SMF quantum Hamiltonian allow us to define in a unique way the approach to equilibrium of the associated classical system, see

Refs. [16, 28, 33], i.e., in a way that zero-temperature, imaginary-time correlation functions of operators diagonal in the SMF basis can be obtained from real-time correlation functions in the stochastic classical system. In particular, if the partition function of the associated classical system undergoes a KT transition upon varying the quantum parameters entering the SMF quantum Hamiltonian, so does the equal-time GS expectation value of operators diagonal in the SMF basis. We can now understand how it is possible to circumvent the no-go theorem. The no-go theorem assumes that a classical phase transition faithfully represents *all* correlation functions in a quantum phase transition with  $z = 1$ . In this paper, only equal-time GS expectation values of operators diagonal in the SMF basis are faithfully represented by correlation functions at the KT critical point since the value of  $z \neq 1$  is not known rigorously. Similar results have been announced by Papanikolaou *et al.* in Ref [50].

The paper is organized as follows. We will show in Sec. 2 that the GS (16)

$$\langle j_0 i \rangle = \frac{1}{\sum_{C \in S_0} e^{\frac{u}{2T} N_C^{(f)}}} \sum_{C \in S_0} C_{ji}$$

of quantum Hamiltonian (13) defines the classical partition function (19) for interacting dimers on the square lattice

$$Z(T=u) = \sum_{C \in S_0} e^{E_C^{(u)} = T}; \quad E_C^{(u)} = u N_C^{(f)} :$$

Here  $S_0$  is the set of all possible classical dimer configurations on the square lattice,  $u$  and  $T$  are two real parameters, and  $N_C^{(f)}$  is the number of plaquettes having two parallel dimers in configuration  $C$ . The classical partition function (19) was studied numerically by Alet *et al.* in Ref. [10] for one sign of the interaction between the dimers. In Sec. 3 we extend the numerical study by Alet *et al.* to the other sign of the interaction between the dimers. The temperature of the classical partition function (19) plays the role of a quantum coupling in the quantum Hamiltonian (13). Ground-state equal-time expectation values of operators diagonal in the dimer basis are thus inherited from the thermodynamics of the classical partition function. In the high-temperature regime, the associated classical system exhibits a line of critical points. As the temperature is lowered, the classical system undergoes either a first-order or KT transition depending on the sign of the interactions between the dimers. To study the robustness of the line of critical points in the zero-temperature phase diagram of quantum Hamiltonian (13), we extend the range of the dimer interactions in Sec. 4. We show that, for one sign of the longer-range dimer interaction, the line of critical points shrinks continuously upon increasing the strength of this longer-range interaction. Section 5 is devoted to another kind of perturbation to our quantum Hamiltonian (13): the presence of defects represented by sites not occupied by a dimer (monomers). We define the more general SMF quantum Hamiltonian (55) that accounts for the existence of monomers in a dilute dimer

model. Once again the GS (56) can be computed exactly

$$\mathcal{Z}_{\text{tot}} = \sum_{C \in \mathcal{S}} e^{(\mu N_C^{(f)} + M_C) = 2T} \mathcal{Z}_C;$$

where, in addition to the quantities defined above,  $\mathcal{S}$  is the set of all classical dilute dimer configurations on the square lattice (i.e., where each site belongs to *at most* one dimer),  $\mu$  is the chemical potential for monomers, and  $M_C$  is the total number of monomers in configuration  $C$ . We can then establish a correspondence between our quantum SMF Hamiltonian and a classical dilute dimer model described by the partition function (57)

$$\mathcal{Z}(T = \mu; \beta = T) = \sum_{C \in \mathcal{S}} \exp \left[ -\frac{E_C(\mu; \beta)}{T} \right] = \sum_{C \in \mathcal{S}} \exp \left[ -\frac{\mu N_C^{(f)} + M_C}{T} \right];$$

This is a promising result as equal-time correlation functions for monomers can thereby be studied, for example, using classical Monte Carlo algorithms [10]. Of course, the computation of unequal-time correlation functions for monomers still requires the use of quantum Monte Carlo simulations or exact diagonalization techniques and is therefore limited to smaller system sizes.

## 2 A square lattice interacting quantum dimer model with solvable ground state

We begin our construction of a quantum square lattice dimer model (SLDM) whose ground state (GS) is exactly solvable by revisiting the quantum dimer model that was introduced by Rokhsar and Kivelson (RK) in Ref. [12]. The Hilbert space is given by the span of the orthonormal basis states  $\mathcal{Z}_C$  labeled by all the classical dimer configurations  $C$  of the square lattice. A classical dimer configuration on the square lattice is obtained by covering all the bonds connecting nearest-neighbor sites with dimers in such a way that each site is the end point of one and only one dimer. The set of all allowed dimer coverings will be denoted by  $\mathcal{S}_0$ .

The RK Hamiltonian acting on this Hilbert space is then commonly written as

$$\hat{H}_{\text{RK}} = \sum_p \left( v \left( \hat{P}_{\text{v}}^{\text{rh}} + \hat{P}_{\text{v}}^{\text{rh}} \right) + t \left( \hat{P}_{\text{h}}^{\text{rh}} + \hat{P}_{\text{h}}^{\text{rh}} \right) \right) \quad (1)$$

where the summation is over all plaquettes  $p$  of the square lattice. The operators  $\hat{P}_{\text{v}}^{\text{rh}}$  and  $\hat{P}_{\text{h}}^{\text{rh}}$  denote projection operators onto the subspace of states associated with configurations  $C$  that contain two parallel dimers (vertical or horizontal, respectively) on plaquette  $p$ . The operators  $\hat{P}_{\text{v}}^{\text{rh}}$  and  $\hat{P}_{\text{h}}^{\text{rh}}$  are the plaquette  $p$  flipping operators that maps any state  $\mathcal{Z}_C$  with two horizontal or

vertical dimers at plaquette  $p$  onto the state  $\overline{\mathcal{C}}_i$  obtained by rotating the two parallel dimers at plaquette  $p$  by 90 degrees, while it annihilates state  $\mathcal{C}_i$  otherwise (i.e., if the configuration  $C$  does not contain two horizontal or vertical parallel dimers at plaquette  $p$ ). Given any classical dimer configuration  $C$ , we shall call any plaquette occupied by two parallel dimers a flippable plaquette.

The representation (1) of the RK Hamiltonian is explicitly local as no reference is made to the dimer covering away from plaquette  $p$  in the definitions of operators  $\hat{J}_{\mathcal{C}_i \mathcal{C}_j}^{\mathbf{r}_p \mathbf{r}_p}$ ,  $\hat{J}_{\mathcal{C}_i \mathcal{C}_j}^{\mathbf{r}_p \mathbf{r}_p}$  and  $\hat{J}_{\mathcal{C}_i \mathcal{C}_j}^{\mathbf{r}_p \mathbf{r}_p}$ ,  $\hat{J}_{\mathcal{C}_i \mathcal{C}_j}^{\mathbf{r}_p \mathbf{r}_p}$ . The nature of the GS of the RK Hamiltonian depends on the dimensionless ratio between the characteristic energies  $v \geq 0$  and  $t \geq 0$ . When  $v=t$ , the GS is expected to display columnar ordering of the dimers, i.e., each dimer has precisely two parallel neighboring dimers. When  $v=t+1$ , the GS is expected to display a staggered ordering of the dimers, i.e., no two parallel neighboring dimers are present in the system. The so-called RK (critical) point

$$v = t \quad (2)$$

in parameter space is special in that the GS is known exactly [12]

$$|j\rangle_i = \sum_{\mathcal{C} \in S_0} \mathcal{C}_i \quad (3)$$

and it is non-degenerate within each irreducible sector of the Hilbert space under the action of the RK Hamiltonian. It separates two ordered phases [36].

The notation used so far is not suitable to construct generalizations of the RK Hamiltonian. What we need instead is a representation that will allow us to “decorate” the plaquettes so as to encode the effects of interactions between dimers beyond just plaquettes with parallel or non-parallel dimers. To this end, let us begin by rewriting the RK Hamiltonian in terms of local objects  $\mathcal{V}_0^{(p)}$  that denote one of the two possible flippable dimer configurations on plaquette  $p$ , i.e., either  $\mathcal{V}_0^{(p)} = \begin{smallmatrix} \text{---} & \text{---} \\ | & | \\ \text{---} & \text{---} \end{smallmatrix}$  or  $\mathcal{V}_0^{(p)} = \begin{smallmatrix} | & | \\ \text{---} & \text{---} \end{smallmatrix}$  (more formally,  $\mathcal{V}_0^{(p)} \in \{\begin{smallmatrix} \text{---} & \text{---} \\ | & | \\ \text{---} & \text{---} \end{smallmatrix}, \begin{smallmatrix} | & | \\ \text{---} & \text{---} \end{smallmatrix}\}$ ). Given the flippable plaquette  $\mathcal{V}_0^{(p)}$  we denote by  $\overline{\mathcal{V}_0^{(p)}}$  the flippable plaquette  $p$  obtained from a 90° rotation of the dimer covering in  $\mathcal{V}_0^{(p)}$  (i.e., if  $\mathcal{V}_0^{(p)} = \begin{smallmatrix} \text{---} & \text{---} \\ | & | \\ \text{---} & \text{---} \end{smallmatrix}$  then  $\overline{\mathcal{V}_0^{(p)}} = \begin{smallmatrix} | & | \\ \text{---} & \text{---} \end{smallmatrix}$ , or if  $\mathcal{V}_0^{(p)} = \begin{smallmatrix} | & | \\ \text{---} & \text{---} \end{smallmatrix}$  then  $\overline{\mathcal{V}_0^{(p)}} = \begin{smallmatrix} \text{---} & \text{---} \\ | & | \\ \text{---} & \text{---} \end{smallmatrix}$ ).

The RK Hamiltonian then becomes

$$\hat{H}_{RK} = \frac{1}{2} \sum_{\mathcal{V}_0^{(p)}} \mathcal{D}_{\mathcal{V}_0^{(p)}} \quad (4)$$

where the sum over the local operators

$$\mathcal{D}_{\mathcal{V}_0^{(p)}} = v \left( \mathcal{J}_0^{(p)} \mathcal{I}_0^{(p)} \mathcal{J}_0^{(p)} + \overline{\mathcal{J}_0^{(p)}} \mathcal{I}_0^{(p)} \overline{\mathcal{J}_0^{(p)}} \right) + t \left( \mathcal{J}_0^{(p)} \mathcal{I}_0^{(p)} \mathcal{J}_0^{(p)} + \overline{\mathcal{J}_0^{(p)}} \mathcal{I}_0^{(p)} \overline{\mathcal{J}_0^{(p)}} \right) \quad (5)$$

runs over all flippable plaquettes. From now on we will drop the explicit dependence on the plaquette index  $p$  in the notation for a flippable plaquette:  $\mathcal{F}_0^{(p)} \rightarrow \mathcal{F}_0$ .

With this notation in hand, one can extend the definition of a flippable plaquette  $\mathcal{F}_0$  to that of a *decorated* flippable plaquette  $\mathcal{F}_0$  in the following way. Whereas  $\mathcal{F}_0$  specifies the position of the plaquette and the orientation of the two parallel dimers covering it,  $\mathcal{F}_0$  contains additional information on the configuration of dimers at neighboring plaquettes. This information can be encoded in a vector  $\mathbf{m} \in \{0,1\}^n$  that lists whether each of  $n$  neighboring bonds is occupied by a dimer or not. For example,  $\mathbf{m} = (m_1; \dots; m_4)$  when the additional information corresponds to specifying whether the four bonds that face the four edges of the plaquette  $p$  are occupied by dimers ( $m_i = 1$ ) or not ( $m_i = 0$ ), as is illustrated in Fig. 1. Given a flippable

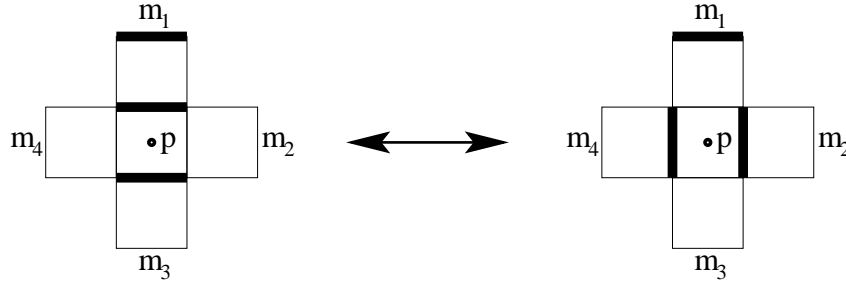


Fig. 1. Example of a local update  $\mathcal{F}_0 \leftrightarrow \overline{\mathcal{F}_0}$  between decorated flippable plaquettes. A decorated flippable plaquette is defined by the choice of the plaquette position  $p$  on the square lattice, by the orientation of the two parallel dimers covering the plaquette  $p$  (e.g., horizontal for  $\mathcal{F}_0$  and vertical for  $\overline{\mathcal{F}_0}$  in this example), and by the values 0 or 1 taken by the four parameters  $m_i$ ,  $i = 1; \dots; 4$  defined on the four bonds that face the four edges of plaquette  $p$ . The value  $m_i = 1$  ( $m_i = 0$ ) corresponds to bond  $i$  being covered (not covered) by a dimer. In this example  $\mathbf{m} = (1; 0; 0; 0)$ .

plaquette  $\mathcal{F}_0$ , the operation  $\mathcal{F}_0 \rightarrow \overline{\mathcal{F}_0}$  is defined by flipping the flippable plaquette  $p$  (see Fig. 1). As before, to any decorated flippable plaquette  $\mathcal{F}_0$  corresponds one and only one  $\overline{\mathcal{F}_0}$ . A straightforward generalization of the RK Hamiltonian (4) then follows by replacing the sum over flippable plaquettes with the sum over decorated flippable plaquettes,

$$\mathcal{H} = \frac{1}{2} \sum_{\mathcal{F}_0} \mathcal{Q}_{\mathcal{F}_0}; \quad (6)$$

where

$$\mathcal{Q}_{\mathcal{F}_0} := v(\mathbf{m}) j_{\mathcal{F}_0}^{\mathcal{F}_0} i_{\mathcal{F}_0} j + \overline{v(\mathbf{m})} j_{\mathcal{F}_0}^{\overline{\mathcal{F}_0}} i_{\overline{\mathcal{F}_0}} j - t(\mathbf{m}) j_{\mathcal{F}_0}^{\mathcal{F}_0} i_{\overline{\mathcal{F}_0}} j + \overline{j_{\mathcal{F}_0}^{\overline{\mathcal{F}_0}} i_{\mathcal{F}_0}} j; \quad (7)$$

This Hamiltonian remains local although now the coupling constants  $v(\mathbf{m}); \overline{v(\mathbf{m})} \in \mathbb{R}$  and  $t(\mathbf{m}) \in \mathbb{R}$  can be used to encode interactions that extend beyond the two parallel dimers at a given flippable plaquette and involve, for example, the four dimers belonging to the four plaquettes that share a bond with plaquette  $p$  in the case of Fig. 1. The GS for generic values of  $v(\mathbf{m}); \overline{v(\mathbf{m})} \in \mathbb{R}$  and  $t(\mathbf{m}) \in \mathbb{R}$  is not known

in closed form. However, when

$$v(m) \overline{v(m)} = t^2(m); \quad t(m) > 0; \quad (8)$$

the GS is given by

$$j_i := \sum_{C \in S_0} C(C) \mathcal{J}_i \quad (9)$$

within any irreducible sector of the Hilbert space under the action of the RK Hamiltonian provided the following integrability condition relating the local data  $v(m)$  and the global expansion coefficient  $C(C)$  holds [33]. For any dimer configuration  $C$  and for any decorated flippable plaquette  $\mathcal{P}_0$  present in  $C$  the dimer configuration,  $\overline{C}$  is uniquely defined by replacing  $\mathcal{P}_0$  with  $\overline{\mathcal{P}_0}$ , while the integrability condition is satisfied whenever

$$C(\overline{C}) = C(C) = \frac{1}{2} (v(m) + t(m) + \overline{v(m)}) \quad (10)$$

holds. The conditions above precisely define the Stochastic Matrix Form (SMF) decomposition of a quantum Hamiltonian discussed in Sec. 1. For the remaining of this section, we will focus on the example of decorated flippable plaquettes depicted in Fig. 1.

The existence of the global expansion coefficients in the GS (9) satisfying the integrability condition (10) can be verified for the choice

$$\begin{aligned} v(m) &= \exp(u N_{\mathcal{P}_0}^{(f)} = 2T); \\ \overline{v(m)} &= \exp(u N_{\overline{\mathcal{P}_0}}^{(f)} = 2T); \\ t(m) &= 1; \end{aligned} \quad (11)$$

with

$$N_{\mathcal{P}_0}^{(f)} = [(m_1 + m_3) - (m_2 + m_4)] = N_{\overline{\mathcal{P}_0}}^{(f)}; \quad (12)$$

Here,  $u = T/2 \in \mathbb{R}$  and the  $+$  ( $-$ ) sign is associated to the vertical (horizontal) orientation taken by the two parallel dimers occupying the flippable plaquette  $\mathcal{P}$  in  $\mathcal{P}_0$ . One verifies that  $N_{\mathcal{P}_0}^{(f)}$  can only assume the values 0,  $\pm 1$ , and  $\pm 2$ . With this choice, the Hamiltonian

$$\mathcal{H}_0 = \frac{1}{2} \sum_{\mathcal{P}_0} \mathcal{Q}_{\mathcal{P}_0} \quad (13)$$

is the sum over (non-commuting) operators with an index running over all decorated flippable plaquettes

$$\mathcal{Q}_{\mathcal{P}_0} = e^{u N_{\mathcal{P}_0}^{(f)} = 2T} \mathcal{J}_0^{\downarrow} i h_0^{\downarrow} \mathcal{J}_0 + e^{u N_{\overline{\mathcal{P}_0}}^{(f)} = 2T} \overline{\mathcal{J}_0^{\downarrow}} i h_0^{\downarrow} \overline{\mathcal{J}_0} - \overline{\mathcal{J}_0^{\uparrow}} i h_0^{\uparrow} \mathcal{J}_0 - \mathcal{J}_0^{\uparrow} i h_0^{\uparrow} \overline{\mathcal{J}_0} \quad (14)$$

each of which is proportional to a projection operator:

$$\mathcal{Q}_{\mathcal{P}_0}^2 = e^{u N_{\mathcal{P}_0}^{(f)} = 2T} + e^{u N_{\overline{\mathcal{P}_0}}^{(f)} = 2T} \mathcal{Q}_{\mathcal{P}_0}; \quad (15)$$



The nodeless wavefunction

$$|j_0\rangle = \sum_{C \in \mathcal{S}_0} e^{\frac{u}{2T} N_C^{(f)}} |C\rangle; \quad (16)$$

where  $N_C^{(f)}$  is the number of flippable plaquettes in the classical dimer configuration  $C$ , is annihilated by the action of each  $\hat{\mathcal{Q}}_0$  for all  $|j_0\rangle$  as follows from verifying that

$$N_{|j_0\rangle}^{(f)} = N_C^{(f)} - N_C^{(f)} : \quad (17)$$

Therefore,  $|j_0\rangle$  is a GS of  $\hat{\mathcal{H}}_0$ , which, with the help of Perron-Fröbenius theorem, can be shown to be *unique* within each *irreducible* sector of  $\hat{\mathcal{H}}_{RK}$  under the action of  $\hat{\mathcal{H}}_0$  [33]. Remarkably, the GS expectation value of any quantum operator  $\hat{\mathcal{O}}$  that is diagonal in the preferred basis  $|C\rangle$  can be written in term of an equilibrium thermal average for a square lattice classical dimer model,

$$\begin{aligned} \frac{\langle j_0 | \hat{\mathcal{O}} | j_0 \rangle}{\langle j_0 | j_0 \rangle} &= \sum_{C \in \mathcal{S}_0} e^{\frac{u}{2T} N_C^{(f)} + N_C^{(f)}} \frac{\langle C | \hat{\mathcal{O}} | C \rangle}{\langle j_0 | j_0 \rangle} \\ &= \frac{1}{Z(T=u)} \sum_{C \in \mathcal{S}_0} e^{\frac{u}{T} N_C^{(f)}} \mathcal{O}_C; \end{aligned} \quad (18)$$

with

$$Z(T=u) = \sum_{C \in \mathcal{S}_0} e^{E_C^{(u)} = T}; \quad E_C^{(u)} = u N_C^{(f)}; \quad (19)$$

and

$$\mathcal{O}_C = \langle C | \hat{\mathcal{O}} | C \rangle; \quad (20)$$

It follows that the zero-temperature phase diagram of the interacting quantum SLDM (13) contains the phase diagram of the interacting classical SLDM (19). The next section is devoted to the numerical study of the phase diagram of the interacting classical SLDM (19).

### 3 The associated classical model

The interacting classical SLDM defined by the partition function (19) has been extensively studied by Alet *et al.* in Ref. [10] for positive values of the coupling constant  $u$ . Notice that in the range  $K = u/T \in (0; 1)$  the classical energy  $E_C^{(u)}$  favors configurations with a large number of flippable plaquettes, while the diagonal term in the quantum Hamiltonian in Eq. (13,14) always penalizes the presence of flippable plaquettes for all values of  $K$ . Conversely, in the range  $K \in (1; \infty)$  the presence of flippable plaquettes is also penalized at the classical level. Configurations with the largest number of flippable plaquettes are referred to as the *columnar* state (every dimer has two parallel neighboring dimers along every other row

or column). A representative among all configurations with no flippable plaquettes is the *staggered* state. A staggered state is obtained from its parent columnar state upon translation of every other dimer of each column, say, by one lattice spacing along the direction parallel to the dimers. For brevity, we will refer to the parameter range  $K > 0$  as the *columnar* side of the interaction, and to the parameter range  $K < 0$  as the *staggered* side of the interaction.

This section is devoted to studying the full parameter range  $K \in (-1; 1)$  of the interacting classical SLDM (19) using transfer matrix techniques. A brief summary of Alet's results is given in Sec. 3.3.1, where we also present our results on the columnar side of the interaction.

### 3.1 The conformal field theory description in the $T = 1$ limit

At infinite temperature ( $K = 0$ ), the partition function (19) reduces to the non-interacting classical SLDM. It exhibits critical spatial correlation functions with power-law decay [3, 4]. The long-wavelength limit of this model is known to be described by the 2D Sine-Gordon field theory whose action can be written in terms of a continuous (height) scalar field  $h$  [13, 5, 6],

$$S = \int d^2r \left[ \frac{g}{2} (\nabla h)^2 + V \cos(2\pi q h) \right]; \quad (21)$$

where  $g$  is called the stiffness and the  $V > 0$  term is called the locking potential. Remarkably, the stiffness and the periodicity of the locking potential are fixed uniquely to the values  $g = 1/2$  and  $q = 4$ , respectively, if the Sine-Gordon action (21) is to encode the long distance asymptotics of the non-interacting SLDM [4, 5, 6]. The scaling dimensions  $d_{e,m}$  of the so-called vertex operators at the free-field fixed point  $V = 0$  of the Sine-Gordon field theory (21) can be classified in terms of their *electric* and *magnetic* charge  $e$  and  $m$ , respectively

$$d_{e,m} = \frac{1}{2} \left( \frac{e^2}{g} + g m^2 \right); \quad e, m \in \mathbb{Z}; \quad (22)$$

The physical interpretation of electric vertex operators is that their correlation functions represent the long distance asymptotics of the dimer correlation functions provided their charge  $e$  is a multiple of  $q = 4$ . The physical interpretation of magnetic vertex operators is that their correlation functions represent the long distance asymptotics of the monomers correlation functions whereby it is understood that monomers are defects in a dimer covering by which sites are not the end points of dimers. Monomers will be introduced at the microscopic level in Sec. 5 but are absent in the present SLDM, i.e.,  $m = 0$  must be enforced. If so, the most relevant electric vertex operator with  $e$  multiple of  $q = 4$  is the locking potential with scaling dimension  $d_{4,0} = 1/6$  in the  $K = 0$  limit. We conclude that the free-field fixed

point  $V = 0$  is the attractive fixed-point of the Sine-Gordon theory (21) if it is to capture the long-distance physics of the non-interacting SLDM.

### 3.2 Construction of the transfer matrix

In order to study the phase diagram of the interacting classical SLDM (19) at finite values of the reduced coupling constant  $K = u=T$ , it is convenient to use a combination of numerical transfer-matrix (TM) calculations in the *infinite-strip geometry* with conformal field theory (CFT) arguments.

We define the interacting classical SLDM (19) on an  $L \times M$ ,  $M \rightarrow \infty$  square lattice and impose periodic boundary conditions in both directions (i.e., wrapped around a torus with infinite principal radius). The width  $L$  must be *even* to respect the bipartite nature of the lattice. The TM  $T^{(L)}$  connects one row of the lattice to the following one along the principal (infinite) axis of the torus, as illustrated in Fig. 2, and satisfies

$$Z(T=u; L; M) = \text{Tr}^{h_i} T^{(L)}(T=u)^{i_M}; \quad (23)$$

where  $Z(T=u; L; M)$  is the partition function of the system. We shall assume (for simplicity) that the TM  $T^{(L)}$  can be diagonalized through a similarity transformation, and we label its (positive) eigenvalues in descending order

$$T^{(L)} = \text{diag} \left( \lambda_0^{(L)}, \lambda_1^{(L)}, \lambda_2^{(L)}, \dots \right); \quad \lambda_0^{(L)} > \lambda_1^{(L)} > \lambda_2^{(L)} > \dots; \quad (24)$$

Anticipating an exponential growth with  $L$  of the TM eigenvalues, we also define the exponents

$$f_n^{(L)} \equiv \frac{1}{L} \ln \lambda_n^{(L)}; \quad n = 0; 1; 2; \dots; \quad (25)$$

The sign is chosen here by convention.

The dimensionless intensive free energy in the thermodynamic limit

$$f(T=u) \equiv \lim_{L \rightarrow \infty} f^{(L)}(T=u; L) \quad (26)$$

is related to the TM  $T^{(L)}$  by

$$f(T=u; L) \equiv \frac{1}{L} \lim_{M \rightarrow \infty} \frac{1}{M} \ln \text{Tr}^{h_i} T^{(L)}(T=u)^{i_M} \quad (27)$$

and is thus solely controlled by the largest (non-degenerate) eigenvalue  $\lambda_0^{(L)}$  of the TM  $T^{(L)}$ ,

$$f(T=u) = \lim_{L \rightarrow \infty} \frac{1}{L} \ln \lambda_0^{(L)}(T=u) = \lim_{L \rightarrow \infty} f_0^{(L)}(T=u; L); \quad (28)$$

If the long wavelength limit of the interacting classical SLDM (19) is captured by a CFT, the central charge of the CFT and the scaling dimensions of the primary fields in the CFT can also be extracted from the finite size ( $L$ ) dependence of the TM  $T^{(L)}$ . The dependence on  $T=u$  of the central charge  $c(T=u)$  is given by

$$f(T=u; L) = f(T=u) - \frac{c(T=u)}{6L^2} + O(L^{-3}); \quad (29)$$

The dependence on  $T=u$  of the scaling dimensions  $d_n(T=u)$  of the CFT primary fields is in turn given by

$$f_n(T=u; L) = f(T=u; L) = \frac{2 d_n(T=u)}{L^2} + O(L^{-3}); \quad n = 1, 2; \quad : \quad (30)$$

We now turn to the explicit construction of the TM  $T^{(L)}$ . To this end, we introduce the variables  $n_i$  on the bonds of the lattice,  $n_i = 0$  (1) if the edge is empty (occupied) by a dimer, as is illustrated in Fig. 2. Any allowed (initial) configuration

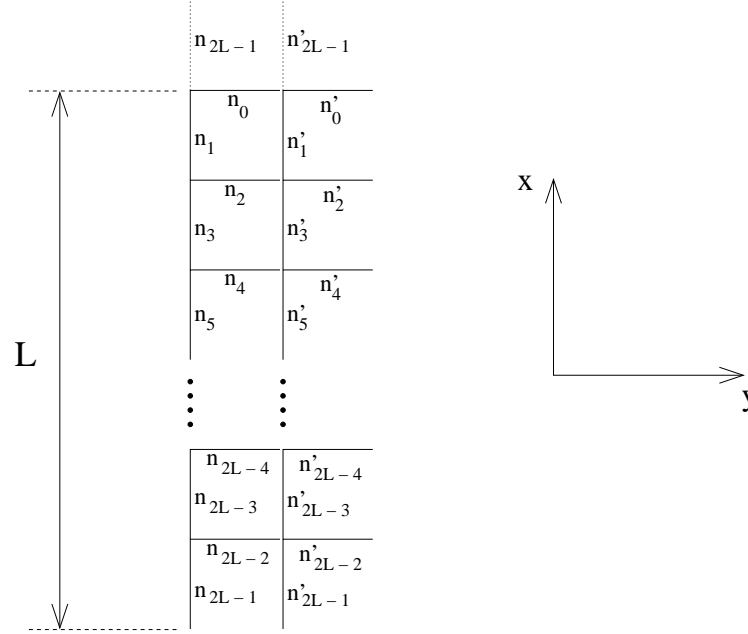


Fig. 2. Labeling of the edge variables  $n_i$  in the TM  $T^{(L)}$ . Periodic boundary conditions are assumed along the  $x$  direction, i.e.,  $n_0 = n_{2L}$ .

$n = f n_i; i = 0; \dots; 2L - 1$  must then satisfy

$$n_{2x-1} + n_{2x} + n_{2x+1} = 1; \quad 0 \leq x \leq L-1; \quad (31)$$

while the TM  $T^{(L)}$  connects only configurations  $n$  and  $n^0$  that satisfy

$$n_{2x-1}^0 + n_{2x}^0 + n_{2x+1}^0 + n_{2x} = 1; \quad 0 \leq x \leq L-1; \quad (32)$$

We can then write

$$T_{n^0, n}^{(L)}(T=u) = T_{n^0, n}^{(L)}(0) U_{n^0, n}^{(L)}(T=u) V_{n^0, n}^{(L)}(T=u); \quad (33)$$

where the two contributions due to the interaction  $U_{n^0, n}^{(L)}(T=u)$  and  $V_{n^0, n}^{(L)}(T=u)$  (accounting for horizontal and vertical parallel dimers, respectively), and the contribution due to the constraint  $T_{n^0, n}^{(L)}(0)$  take the form

$$\begin{aligned} T_{n^0, n}^{(L)}(0) &= \prod_{x=1}^L (n_{2x-1}^0 + n_{2x}^0 + n_{2x+1}^0 + n_{2x}^0 - 1); \\ U_{n^0, n}^{(L)}(T=u) &= \exp \left[ \frac{u}{T} \sum_{x=0}^{L-1} \frac{n_{2x} n_{2x+2} + n_{2x}^0 n_{2x+2}^0}{2} \right]; \\ V_{n^0, n}^{(L)}(T=u) &= \exp \left[ \frac{u}{T} \sum_{x=0}^{L-1} n_{2x+1} n_{2x+1}^0 \right]; \end{aligned} \quad (34)$$

respectively.

The computational effort to obtain the eigenvalues of the TM  $T^{(L)}$  can be reduced by looking for quantities that are left invariant under the action of the TM. This allows to block diagonalize  $T^{(L)}(T=u)$  and to compute the largest eigenvalues separately in each sector. As discussed in Ref. [10] and using the notation defined in Fig. 2, one can show that the quantity

$$W_x = \prod_{i=0}^{L/2-1} (n_{4i} n_{4i+2} - 2) \quad \frac{L}{2}; \dots; \frac{L}{2} \quad (35)$$

is conserved as one proceeds along the  $y$ -axis through repeated applications of the TM. One can thus use  $W_x$  to label the diagonal blocks of  $T^{(L)}(T=u)$ . Observe that any block with  $W_x \neq 0$  corresponds to having  $|W_x|$  monomers on the same sublattice at  $y = -1$ , and  $|W_x|$  monomers on the opposite sublattice at  $y = 1$ , as discussed in Ref. [10]. We will impose the condition that there are no monomers, i.e.,  $W_x = 0$ , when considering the electrical sector of the CFT in isolation. We shall assume that, upon ordering the eigenvalues of the TM within each sector according to

$$\lambda_0^{(W_x; L)} \geq \lambda_1^{(W_x; L)} \geq \dots; \quad (36)$$

$\lambda_0^{(0; L)}$  is the global maximal TM eigenvalue. If so, it is  $\lambda_0^{(0; L)}$  that controls the free energy and central charge of the system following Eq. (28) and Eq. (29) (with the possible exception of the transition to the staggered phase, as discussed in Sec. 3.3.2). In Sec. 4.1 we show how the introduction of longer-range couplings in the dimer model gives rise to new phase transitions that are not entirely captured by the  $W_x = 0$  sector, and one needs to compute the largest eigenvalue from the global TM. We shall also define the exponents

$$f_n^{(W_x)}(L) \equiv \frac{1}{L} \ln \lambda_n^{(W_x; L)}; \quad n = 0; 1; 2; \quad (37)$$

within each irreducible sector. Equation (30) together with Eq (22) imply that the ratio  $\frac{\chi_0^{(0;L)}}{\chi_1^{(0;L)}} = \frac{\chi_0^{(0;L)}}{\chi_1^{(0;L)}}$  determines the scaling dimension  $d_{1;0}$  while the ratio  $\frac{\chi_0^{(0;L)}}{\chi_0^{(1;L)}} = \frac{\chi_0^{(0;L)}}{\chi_0^{(1;L)}}$  determines the scaling dimension  $d_{0;1}$ . From the values of either of these two scaling dimensions one obtains the stiffness  $g$  of the CFT of Eq. (21), and therefore the scaling dimensions of all the operators in the theory. Measuring both of them allows for a further check on the reliability of the numerical results, as the product of  $d_{0;1}$  and  $d_{1;0}$  must remain constant even if  $g$  varies ( $d_{0;1} d_{1;0} = 1/4$ ).

### 3.3 The transfer matrix results

Exploiting the sparse nature of the TM due to the constraint-enforcing term  $T_{n_0 n_1}^{(L)}(0)$ , we compute its largest eigenvalues using a combination of hashing techniques to encode the state space of the system and routines from the ARPACK library [51] based on the implicitly restarted Arnoldi method (or implicitly restarted Lanczos method, whenever applicable), which are particularly suitable to handle large sparse matrices. Specifically, we compute the largest and first subleading eigenvalues of the TM in the  $W_x = 0$  sector, as well as the largest eigenvalue of the TM in the  $W_x = 1$  sector. This allows us to obtain, from finite size scaling, the dimensionless intensive free energies  $f_0^{(0)}$  and  $f_0^{(1)}$  in the sectors  $W_x = 0$  and  $W_x = 1$ , respectively, the central charge  $c$ , and the scaling dimensions  $d_{1;0}$  and  $d_{0;1}$  of the electric and magnetic vertex operators, respectively. We also compute the global largest and first subleading eigenvalues of the TM, i.e., independently of the value of  $W_x$ . We can thus verify that the global dimensionless intensive free energy and the central charge are indeed controlled by  $f_0^{(0)}$ .

For each value of the reduced coupling constant  $K = u/T$  and in each block-diagonal sector, we consider systems of size  $L = 6; 8; 10; 12; 14; 16$ . We then use standard finite-size scaling techniques [52] to extrapolate the desired quantities. Namely, we fitted the computed values

$$\begin{aligned} f_0^{(0)}(L) &= \frac{1}{L} \ln(\chi_0^{(0;L)}); \\ f_1^{(0)}(L) \quad f_0^{(0)}(L) &= \frac{1}{L} \ln(\chi_1^{(0;L)}) \quad \ln(\chi_0^{(0;L)})^{\frac{1}{L}}; \\ f_0^{(1)}(L) \quad f_0^{(0)}(L) &= \frac{1}{L} \ln(\chi_0^{(1;L)}) \quad \ln(\chi_0^{(0;L)})^{\frac{1}{L}}; \end{aligned} \quad (38)$$

for  $L = 6; 8; 10; 12; 14; 16$ , with the scaling forms

$$\begin{aligned} f &= \frac{c}{6L^2} + \frac{A}{L^4}; \\ \frac{2}{L^2} d_{1;0} &+ \frac{A}{L^4}; \\ \frac{2}{L^2} d_{0;1} &+ \frac{A}{L^4}; \end{aligned} \quad (39)$$

respectively. The  $1=L^4$  term is introduced to speed up the convergence of the fitting routine for the parameters  $c$ ,  $d_{1,0}$ , and  $d_{0,1}$  [52]. Specifically, we first obtain *estimates* of the above parameters by fitting data points with  $L_0 = L_{\max}$ , where  $L_{\max} = 16$  is the largest strip width that we consider, and  $L_0$  is varied from 6 to  $L_{\max} - 4$  ( $L_{\max} - 2$  in the case of the scaling exponents). The resulting estimants  $c(L_0; L_{\max})$ ,  $d_{1,0}(L_0; L_{\max})$ , and  $d_{0,1}(L_0; L_{\max})$  are given in Tables 1, 2, and 3. We then extrapolated the estimants in the limit  $L_0 \rightarrow 1$  by assuming the power law form [52]

$$x(L_0; L_{\max}) = x + kL_0^p; \quad (40)$$

for each of the three quantities  $x = c; d_{1,0}; d_{0,1}$ , and performing an appropriate fit of the data in Tables 1, 2, and 3. Whenever the last three estimants in a row of Tables 1, 2, and 3 appear in monotonically decreasing order, they are used to obtain the constants  $x$ ,  $k$ , and  $p$ . When this is not the case, or whenever the power  $p$  obtained from the fit is too small to produce a reliable extrapolation (namely if  $p < 1$ , from experience), then the Ising-like value  $p = 2$  is assumed and only the last two estimants are considered for the fit to obtain  $x$  and  $k$  (denoted by a  $(\cdot)$  in the Tables 1, 2, and 3) [52]. A rough estimate for the error bar can be obtained by considering the variation among the estimants [52]. In the results shown in Figs. 3-6, the error bars are computed as the square root of the variance of the last three estimants used for the extrapolation. In most cases, the error bars are smaller than the symbols used in the plots.

The results for the central charge and scaling exponents are shown in Figs. 3 and 4, for the columnar and staggered side of the interaction respectively.

The same fitting approach is used to extrapolate the global free energy  $f$  from its estimants  $f(L_0; L_{\max})$ , as well as  $f^{(0)}$  (in the sector  $W_x = 0$ ) and  $f^{(1)}$  (in the sector  $W_x = 1$ ). The data are omitted here for brevity, and we show only the results for the staggered side in Fig. 6.

### 3.3.1 The columnar side

On the columnar side of the interaction (Fig. 3), our results are in good agreement with the ones obtained by Alet *et al.*. The system remains critical for small but finite values of the reduced coupling  $K = u/T$  up to some critical value in the range  $(1.5; 1.7)$  (compare with the critical temperature  $T_c^{(\text{columnar})} = 0.65u$  in Ref. [10]) and its long wavelength limit is described by the CFT (21) with continuously varying stiffness  $g = 2\phi_{\beta,1}$ . In the limit of  $K \rightarrow 0$ , one recovers the expected value  $g = 1/2$  (not shown) and the cosine term is irrelevant as  $d_{4,0} = 8/g = 16$ . When the value of  $K$  is increased, the stiffness increases monotonically and the scaling dimension of the cosine term decreases correspondingly, until this operator becomes marginal at  $T = T_c^{(\text{columnar})}$  ( $d_{4,0} = 2$ ,  $g = 4$ ). The system undergoes then a Kosterlitz-Thouless (KT) transition into the columnar ordered phase, as confirmed by the Monte Carlo simulation results presented in Ref. [10].

Table 1

List of the estimants  $c(L_0; L_{\max})$  obtained from parabolic fits in  $1=L^2$  for all the values of  $K = u/T$  considered in this paper. The error bar on the extrapolated value is obtained from the variation among the estimants used in the corresponding extrapolation.

K	$c(6;16)$	$c(8;16)$	$c(10;16)$	$c(12;16)$	Extrapolation	
1.7	0.9642	0.9510	0.9445	0.9380	0.923	0.005
1.5	1.0135	1.0083	1.0099	1.0101	1.010	0.001
1.0	0.9900	0.9885	0.9924	0.9966	1.006	0.003
0.7	0.9904	0.9886	0.9925	0.9966	1.006	0.003
0.5	0.9906	0.9889	0.9923	0.9960	1.004	0.003
0.4	0.9907	0.9891	0.9922	0.9955	1.003	0.003
0.35	0.9910	0.9893	0.9934	0.9953	0.998	0.002
0.0	0.9947	0.9919	0.9951	0.9979	1.004	0.002
-0.1	0.9959	0.9926	0.9950	0.9968	1.001	0.002
-0.22	0.9974	0.9935	0.9944	0.9960	1.000	0.001
-0.35	0.9985	0.9938	0.9952	0.9985	1.006	0.002
-0.5	0.9991	0.9937	0.9951	0.9993	1.009	0.002
-0.7	0.9963	0.9923	0.9932	0.9947	0.9981	0.001
-1.0	0.9507	0.9716	0.9808	0.9864	1.005	0.006
-1.12	0.8998	0.9401	0.9617	0.9741	1.007	0.01
-1.28	0.7890	0.8563	0.8990	0.9276	0.99	0.03
-1.5	0.5719	0.6472	0.7047	0.7491	0.85	0.04
-2.0	0.2676	0.2765	0.2896	0.2991	0.321	0.009
-3.0	-0.0118	-0.0086	-0.0063	-0.0068	-0.008	0.001
-4.0	0.0012	-0.0006	-0.0001	-0.0001	-0.0001	0.0002

Notice that, contrary to the RK model in Eq. (1) [36], in our quantum model the presence of a possible resonating plaquette phase seems to be excluded according to the Monte Carlo results by Alet *et al.* [10].

### 3.3.2 The staggered side

On the staggered side of the interaction (Fig. 4), the central charge remains again constant at  $c = 1$  for small but finite values of the reduced coupling  $K$ , until it



Table 2

List of the estimants  $d_{1,0}(L_0; L_{\max})$  obtained from parabolic fits in  $1=L^2$  for all the values of  $K = u/T$  considered in this paper. The error bar on the extrapolated value is obtained from the variation among the estimants used in the corresponding extrapolation.

K	$d_{1,0}(8;16)$	$d_{1,0}(10;16)$	$d_{1,0}(12;16)$	$d_{1,0}(14;16)$	Extrapolation	
1.7	0.0878	0.0838	0.0806	0.0779	0.071	0.002
1.5	0.1489	0.1483	0.1478	0.1475	0.1465	0.0003
1.0	0.3095	0.3090	0.3087	0.3084	0.3076	0.0003
0.7	0.4352	0.4350	0.4348	0.4347	0.4344	0.0001
0.5	0.5454	0.5458	0.5461	0.5462	0.5467	0.0002
0.4	0.6120	0.6128	0.6132	0.6135	0.6141	0.0003
0.35	0.6488	0.6498	0.6504	0.6507	0.6517	0.0004
0.0	0.9986	0.9993	0.9995	0.9997	0.9998	0.0002
-0.1	1.1384	1.1381	1.1379	1.1379	1.1379	0.0001
-0.22	1.3375	1.3362	1.3359	1.3358	1.3358	0.0001
-0.35	1.5979	1.5998	1.6008	1.6012	1.6016	0.0006
-0.5	1.9848	1.9984	2.0018	2.0026	2.003	0.002
-0.7	2.1119	2.1336	2.1066	2.0768	1.99	0.02
-1.0	1.9315	2.1446	2.3038	2.4152	3.0	0.1
-1.12	1.7082	1.9126	2.0810	2.2189	2.6	0.1
-1.28	1.4078	1.5727	1.7151	1.8366	2.2	0.1
-1.5	1.0517	1.1546	1.2495	1.3323	1.56	0.07
-2.0	0.4538	0.4469	0.4471	0.4499	0.453	0.001
-3.0	0.9469	0.9481	0.9534	0.9605	0.980	0.005
-4.0	1.6293	1.6312	1.6326	1.6340	1.638	0.001

abruptly drops to zero at some critical value in the range  $(-1.5; -1.28)$ . We can therefore estimate the critical temperature for the transition to the staggered phase to be  $T = T_c^{(\text{staggered})} \approx (-0.72 \pm 0.05)u$ . The system remains critical for temperatures above  $T_c^{(\text{staggered})}$  while the stiffness  $g$  decreases monotonically with decreasing  $T$ , as signaled by the behavior of the scaling dimensions  $d_{1,0}$  and  $d_{0,1}$ .

Notice that, on this side of the interaction, all the allowed operators with zero magnetic charge (i.e., those with  $e = 4n$ ,  $n = 1; 2; \dots$ ) have scaling dimensions  $d_{e,0}$  larger than two. The absence of an allowed operator that becomes relevant for

Table 3

List of the estimants  $d_{0;1}(L_0;L_{\max})$  obtained from parabolic fits in  $1=L^2$  for all the values of  $K = uT$  considered in this paper. The error bar on the extrapolated value is obtained from the variation among the estimants used in the corresponding extrapolation.

K	$d_{0;1}(8;16)$	$d_{0;1}(10;16)$	$d_{0;1}(12;16)$	$d_{0;1}(14;16)$	Extrapolation	
1.7	1.8139	1.9017	1.9671	2.0186	2.16	0.05
1.5	1.4269	1.4689	1.4972	1.5175	1.57	0.02
1.0	0.8044	0.8095	0.8121	0.8136	0.817	0.002
0.7	0.5735	0.5747	0.5752	0.5755	0.5759	0.0003
0.5	0.4562	0.4567	0.4569	0.4570	0.4572	0.0001
0.4	0.4061	0.4064	0.4066	0.4067	0.4067	0.0001
0.35	0.3829	0.3832	0.3833	0.3834	0.3835	0.0001
0.0	0.2494	0.2497	0.2498	0.2498	0.2499	0.0001
-0.1	0.2191	0.2194	0.2195	0.2196	0.2196	0.0001
-0.22	0.1865	0.1868	0.1869	0.1870	0.1871	0.0001
-0.35	0.1554	0.1557	0.1558	0.1559	0.1559	0.0001
-0.5	0.1243	0.1246	0.1248	0.1248	0.1249	0.0001
-0.7	0.0901	0.0902	0.0904	0.0905	0.0908	0.0001
-1.0	0.05186	0.05166	0.05164	0.05164	0.05164	0.00001
-1.12	0.0404	0.0400	0.0399	0.0399	0.0398	0.0001
-1.28	0.0279	0.0275	0.0273	0.0271	0.0266	0.0002
-1.5	0.0089	0.0110	0.0147	0.0145	0.014	0.002
-2.0	-0.0099	-0.0005	-0.0052	-0.0042	-0.001	0.002
-3.0	-0.0011	-0.0003	0.0002	0.0002	0.0001	0.0003
-4.0	0.00008	0.00002	0.00000	0.00000	0.00000	0.00001

$T > T_c^{(\text{staggered})}$  is consistent with the transition being first order, as expected in analogy with the RK Hamiltonian [12] (see also the results on the free energy presented below).

Finally, the stiffness  $g$  seems to vanish exactly at the staggered transition (within numerical error), suggesting that a tilting transition occurs at  $T_c^{(\text{staggered})}$  as briefly noted in Ref. [10]. Observe, however, that our estimate  $T_c^{(\text{staggered})} = 0.72(0.05)u$  differs from the estimate  $T_c^{(\text{staggered})} = 0.449(1)u$  in Ref. [10]. A possible explanation for this discrepancy might be due to strong topology-dependent finite-

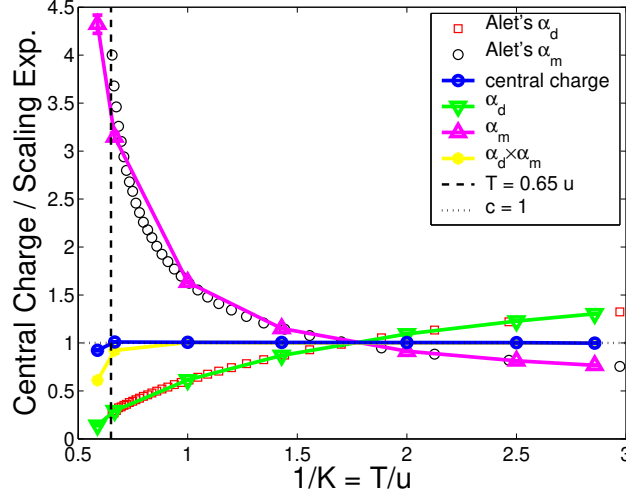


Fig. 3. Central charge and scaling exponents for the electric and magnetic monopole operators on the columnar side of the interaction. Following the convention in Ref. [10], we plot the scaling exponents  $\alpha_d = 2d_{1,0}$  and  $\alpha_m = 2d_{0,1}$  (equal to  $1=g$  and  $g$  from Eq. (22), respectively), instead of the scaling dimensions  $d_{e,m}$ . The results by Alet *et al.* are also shown for comparison [10].

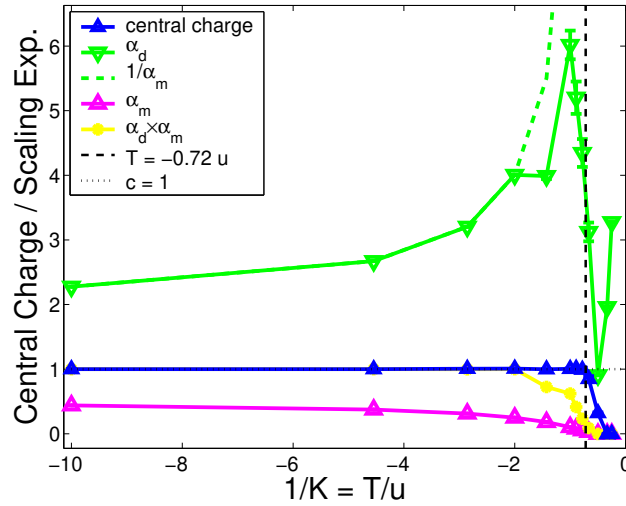


Fig. 4. Central charge and scaling exponents for the electric and magnetic monopole operators on the staggered side of the interaction. Following the convention used in Ref. [10], we plot the scaling exponents  $\alpha_d = 2d_{1,0}$  and  $\alpha_m = 2d_{0,1}$  (equal to  $1=g$  and  $g$  from Eq. (22), respectively), instead of the scaling dimensions  $d_{e,m}$ . The divergence of  $\alpha_d$  close to  $T=0$  makes it increasingly difficult to obtain a reliable extrapolation for  $L \rightarrow 1$ , hence the large fluctuations observed. The smaller parameter  $\alpha_m$  is much less affected and the curve  $1/\alpha_m$  can be used as a guide to the eye for the diverging behavior of  $\alpha_d$ .

size effects. For example, the central charge of the system computed using the global transfer matrix as is done in Fig. 5 suggests a drop of the central charge at the much lower value of  $0.3u$  than the value  $0.72u$  extracted from Fig. 4. In turn, this suggests a strong dependency on the topological sectors of the finite-size

estimate for the critical temperature. Understanding this interplay between finite-size effects and topological sectors is beyond the scope of this paper.

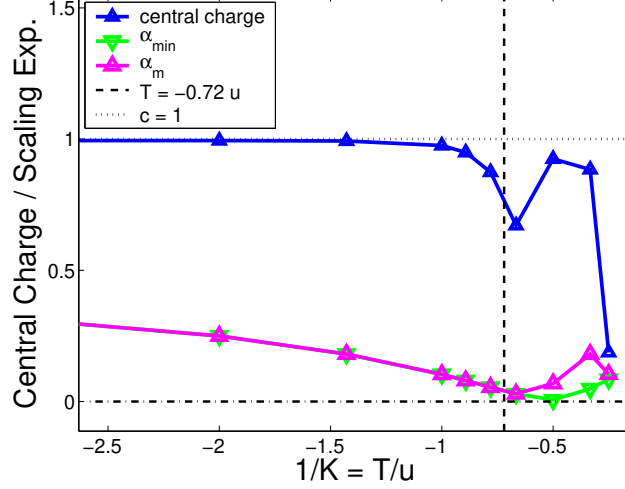


Fig. 5. Estimants of the central charge and scaling exponent for the magnetic monopole operator on the staggered side of the interaction, derived using the global transfer matrix for  $L = 8;12;16$  [53]. Following the convention used in Ref. [10], we plot the scaling exponents  $\alpha_d = 2d_{1,0}$  and  $\alpha_m = 2d_{0,1}$  (equal to  $1-g$  and  $g$  from Eq. (22), instead of the scaling dimensions  $d_{em}$ . For comparison, we also show the estimants of  $\alpha_{\min} = 2d_{\min}$  corresponding to the most relevant operator in the CFT, obtained from the first subleading eigenvalue of the global TM. As expected,  $\alpha_m = \alpha_{\min}$  as long as the CG description in Sec. 3.1 holds, i.e., for  $T = u > T_c^{(\text{staggered})}$ .

### 3.3.3 The free energy

The results for the global free energy of the system ( $\mathcal{F}$ ) and for the constrained free energies in the  $w_x = 0$  ( $\mathcal{F}_0^{(0)}$ ) and  $w_x = 1$  ( $\mathcal{F}_0^{(1)}$ ) sectors are shown in Fig. 6 for the staggered side of the interaction. The continuous KT transition on the columnar side is in general difficult to detect from free energy measurements, and the curves (not shown) are indeed smooth and featureless across  $T_c^{(\text{columnar})}$ .

On both sides of the interaction and for the range of temperatures considered here, the three free energies are indistinguishable ( $\mathcal{F} = \mathcal{F}_0^{(0)} = \mathcal{F}_0^{(1)}$ ). This overlap is indeed expected since the number of  $w_x$  sectors is linear in system size, and the presence of defects at  $y = 1$  should not affect significantly the entropy of each sector.

As mentioned above, the transition on the staggered side is expected to be first order. In fact, not only has the set of all possible staggered configurations vanishing entropy, but they also do not allow for local fluctuations (without violating the dimer constraint), so that even the set of all the configurations connected to a staggered one through a single thermal fluctuation has vanishing entropy. This peculiar

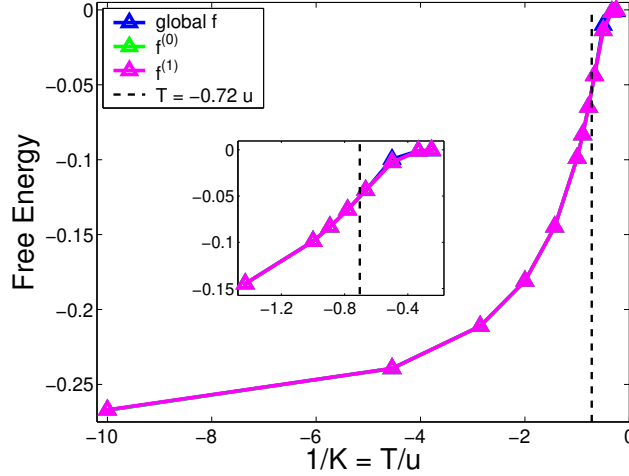


Fig. 6. Free energy of the system obtained from the global TM and from the TM restricted to the  $\bar{W}_x = 0$  and  $\bar{W}_x = 1$  sectors, respectively, for the staggered side of the interaction. The inset shows a close-up view of the temperature range where the transition is expected to happen, and the dashed line indicates the value of  $T_c^{(\text{staggered})}$  predicted from CFT arguments in Sec. 3.3.2.

connectivity of phase space close to the staggered phase leaves little room for a possible continuous phase transition, and indeed in the RK Hamiltonian (1) the transition to the staggered phase is similarly observed to be first order.

The accuracy in our data does not allow for a precise identification of the transition temperature from the free energy plot. However, the overall behavior is in agreement with the value of  $T_c^{(\text{staggered})}$  obtained from CFT considerations, as shown in the inset in Fig. 6 (notice that the staggered phase has both vanishing entropy and vanishing energy, therefore a lower bound for the transition temperature is obtained from the location of the point where the free energy first vanishes). A deeper insight on the nature of this transition could perhaps be obtained from Monte Carlo simulations, even though the non-local nature of the thermal fluctuations above the staggered phase are likely to lead to dynamical slowing down and glassiness, as observed in similar coloring models [54]. A variational (cluster) mean field approach [55, 54] may prove more powerful in obtaining an accurate estimate of the transition temperature to compare with the one from CFT arguments. Such analysis is however beyond the scope of the present paper.

An intriguing question about this transition to the staggered phase would be to understand what happens in this model to the so-called devil's staircase scenario, proposed in the original Rokhsar-Kivelson square lattice dimer model (1) [26].

#### 4 Stability of the critical line

The question that we want to address in this section is how stable is the critical segment  $1=0.72 \leq u=T \leq 1=0.65$  in the zero-temperature phase diagram of the interacting quantum SLDM (13) to a perturbation by some longer-range interaction  $E_C^{(J)}$  between dimers. In order to address this question, at least from a qualitative point of view, we need to substitute

$$E_C^{(u)} \rightarrow E_C^{(u)} + E_C^{(J)} \quad (41)$$

in the classical partition function (19) by retracing all the steps that lead from the interacting quantum SLDM (13) to the classical partition function (19). (That this is possible was proven in Ref. [33].) For the sake of concreteness, let us consider the case where the new contribution to the classical energy of a dimer configuration  $C$  is given by

$$E_C^{(J)} = \frac{J}{2} \sum_i \sum_{h,v} n_i^{(0)} n_i^{(h)} + n_i^{(2)} + n_i^{(3)} + n_i^{(4)} + n_i^{(5)} + n_i^{(6)} \quad (42)$$

Here, the sum over  $i$  runs over all lattice sites, the sum over  $h, v$  runs over the occupation number by horizontal and vertical dimers respectively, and  $n_i^{(r)} = 1$  ( $0$ ),  $r = 0, \dots, 6$  if the bonds depicted in Fig. 7 are covered (not covered) by a dimer. Notice that the  $J$  interaction is comprised of a nearest-neighbor part

$$n_i^{(0)} n_i^{(2)} + n_i^{(0)} n_i^{(5)}$$

and of a next-nearest-neighbor part

$$n_i^{(0)} n_i^{(1)} + n_i^{(0)} n_i^{(3)} + n_i^{(0)} n_i^{(4)} + n_i^{(0)} n_i^{(6)}$$

that are equally weighted. Therefore, varying both  $u$  – which corresponds to a pure nearest-neighbor interaction between dimers – and  $J$  is equivalent to tuning separately the nearest-neighbor and next-nearest-neighbor couplings between dimers. In the limit  $J=T \rightarrow J \neq T$ , the coupling  $J$  favors dimer configurations where the dimers are mostly aligned along the same direction. In this limit, the disordered critical phase between the two ordered phases is penalized. For this reason we conjecture that the effect of an increasing value of  $J=T > 0$  is to shrink continuously the size of the critical segment  $1=0.72 \leq u=T \leq 1=0.65$  at  $J = 0$  until the critical value  $(J=T)_c$  is reached at which the critical line terminates into a tricritical point. A similar behavior is observed in the classical phase diagram of the three-coloring model in presence of an Ising interaction and of a uniform magnetic field [55]. This scenario is depicted in Fig. 8. Beyond this point, i.e., for  $J=T > (J=T)_c$ , we conjecture that the columnar and staggered phases are separated by a first-order phase transition. The slope of the line of first-order transition points for  $J=T > (J=T)_c$  is positive because the  $J > 0$  coupling favors the staggered phase over the columnar

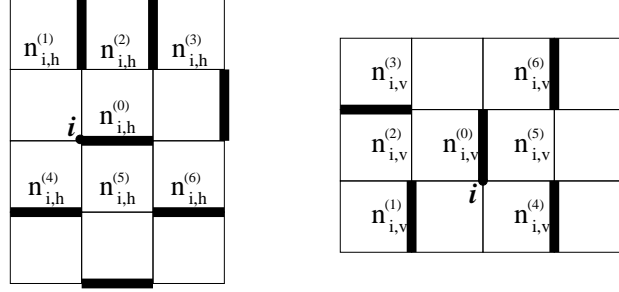


Fig. 7. Given any site  $i$  of the square lattice, the locations of the horizontal bond variables  $n_{i,h} \equiv n_{i,h}^{(0)}; \dots; n_{i,h}^{(6)}$  and the locations of the vertical bond variables  $n_{i,v} \equiv n_{i,v}^{(0)}; \dots; n_{i,v}^{(6)}$  are defined in the left and right panel, respectively. Observe that the right panel is obtained from the left panel after a  $\pi/2$  counterclockwise rotation followed by the substitution  $h \rightarrow v$ . Given the lattice site  $i, r \in \{0; \dots; 6\}$ , and  $2 \leq h, v \leq 6$ , the bond variable  $n_{i,r}^{(x)}$  takes the value 1 if a horizontal ( $x = h$ ) or vertical ( $x = v$ ) dimer is present while  $n_{i,r}^{(x)} = 0$  otherwise. The contribution from site  $i$  to the classical energy  $E_C^{(J)}$  defined in Eq. (42) is  $-J$  for the dimer covering  $C$  in the left panel and  $-3J/2$  for the dimer covering  $C$  in the right panel.

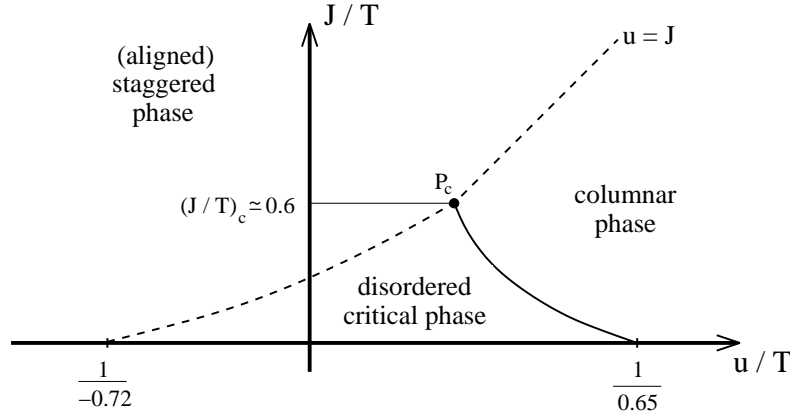


Fig. 8. Phase diagram of the dimer model with both plaquette counting ( $u$ ) and short-range aligning ( $J$ ) interactions. The dashed line delimiting the staggered phase is expected to be a coexistence line (a first-order phase transition), while the solid line between the columnar and the disordered critical phase is expected to be a line of KT (infinite order) transition points. The quantitative details shown here are derived from numerical and analytical arguments in Sec. 4.1. Notice that the phase diagram of a classical system with fixed values of  $u$  and  $J$  as a function of temperature is described by a straight line that passes by the origin of the axes.

phase. The point  $P_c$ , where the continuous KT phase transition to the columnar phase meets the first order phase transition to the staggered phase, is reminiscent of the RK critical point (2) in the RK Hamiltonian (1) in that the transition is first order on one side and continuous on the other side [56].

These conjectures have been tested numerically with the help of transfer matrix

calculations of the central charge and scaling exponents for the system in presence of the additional energy term  $E_c^{(J)}$  in Eq. (42). The numerical techniques that we shall use follow step by step those described in Sec. 3, provided we introduce two extra factors  $\mathcal{U}_{n^0_m}^{(L)} (T=J)$  and  $\mathcal{V}_{n^0_m}^{(L)} (T=J)$  in Eq. (33),

$$\begin{aligned} \mathcal{U}_{n^0_m}^{(L)} (T=J) = & \exp \left[ \frac{J}{T} \sum_{x=0}^{L-1} \frac{n_{2x}}{2} \right. \\ & \left. (1 - n_{2x-1} + n_{2x-2} + n_{2x-3}) + n_{2x-2} + n_{2x-2}^0 \right. \\ & \left. + (1 - n_{2x+1} + n_{2x+2} + n_{2x+3}) + n_{2x+2} + n_{2x+2}^0 \right] ; \\ \mathcal{V}_{n^0_m}^{(L)} (T=J) = & \exp \left[ \frac{J}{T} \sum_{x=0}^{L-1} n_{2x+1} - n_{2x-1}^0 + n_{2x+1}^0 + n_{2x+3}^0 \right] ; \end{aligned} \quad (43)$$

for horizontal and vertical dimers respectively. The notation used here for the labeling of the bonds in the lattice is the same as in Sec. 3.2 (see Fig. 2). The results obtained from these numerical calculations are summarized in Sec. 4.1 and are in agreement with the conjectured phase diagram in Fig. 8.

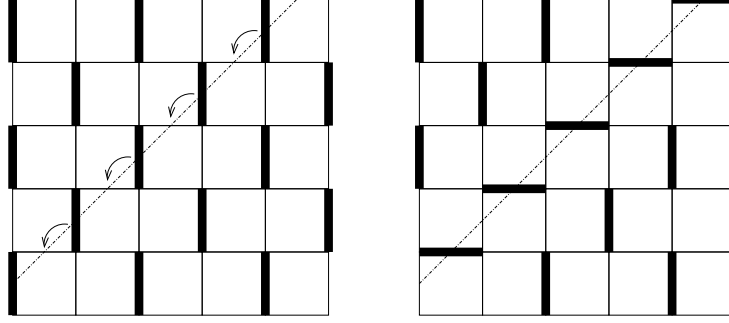
#### 4.1 Numerical results

We ran transfer matrix simulations at fixed values of  $J=T = 0.2; 0.2; 0.5; 1.0$ , and  $1.5$ , while varying  $u=T$  along the same set of values used for the  $J = 0$  case. We also sampled the line  $u = J (= 1)$  in parameter space, at different (inverse) temperatures  $1/T = 0; 0.1; 0.2; 0.3; 0.4; 0.5; 0.7; 1.0; 1.2; 1.5; 1.7; 2.0; 2.5; 3.0$ .

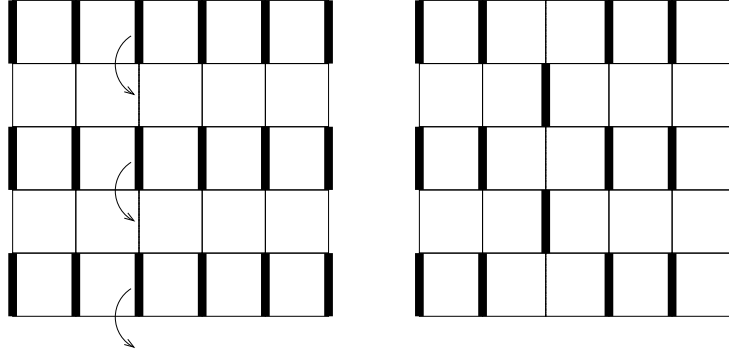
Before presenting the numerical results, let us discuss the low-temperature asymptotics of the system for which analytical arguments can be formulated. For the sake of simplicity we will discuss here the case of an  $L \times L$  square lattice, which one can then generalize to the  $M \times L$  case appropriate for TM calculations. As before,  $L$  is chosen even when imposing periodic boundary conditions so as to maintain bipartiteness of the square lattice.

We begin by considering the case of  $u=T = 1$  and  $J=T = 0$  when the system lies deep within the staggered phase. The degeneracy of the classical ground state manifold in the staggered phase is *subextensive*, in the sense that the number of degenerate configurations is exponential in the *linear* size of the system. To see this start from the staggered configuration defined in the left panel of Fig. 9(a). Draw a line that crosses the mid-points of the occupied bonds along a diagonal, as illustrated in the figure. Given the staggered configuration in the left panel of Fig. 9(a), and imposing periodic boundary conditions, there are  $L/2$  such diagonals (recall that  $L$  must be even to ensure bipartiteness). For any such diagonal line, we are free to take the dimers that intersect the diagonal and rotate them by  $\pi/2$





(a) Staggered phase degeneracy for  $J = 0$



(b) Columnar phase degeneracy for  $u = J$

Fig. 9. Examples of ordered phases in the asymptotic limits  $u=T \rightarrow 1$ ;  $J = 0$  (Top) and  $u=T$ ;  $J=T \rightarrow 1$  (Bottom). For  $J = 0$  all staggered configurations are degenerate, and can be obtained from the four canonical configurations – one of which is shown in the Top-left figure – by  $\pi$ -degree rotation of the dimers along diagonals (Top-right). Equivalently, for  $u = J$  all configurations obtained from one of the four columnar states by one-sublattice translations of rows of collinear dimers (Bottom-left & Bottom-right) are also degenerate.

without violating the dimer constraint or creating flippable plaquettes, as it has been done on the right panel of Fig. 9(a). Hence, both configurations depicted in Fig. 9(a) are degenerate in energy when  $J=T = 0$ . By global  $\pi$ -rotations of all the bonds intersecting any one of the  $L=2$  diagonals, one generates a total of  $2^{L=2}$  degenerate configurations when  $J=T = 0$  [57]. This degeneracy equals the number of all possible Ising spin configurations along a chain made of  $L=2$  sites. Notice that we could have equivalently well chosen a top-left to bottom-right diagonal instead of a top-right to bottom-left diagonal as illustrated in Fig. 9(a). This choice can be shown to generate another  $2^{L=2}$  degenerate configurations, only one of which has already been counted before (for a total of  $2 \cdot 2^{L=2} - 1$ ). Similarly, one can show that if we take as the starting configuration the one that obtains from the left panel of Fig. 9(a) by means of a translation by one lattice spacing in the horizontal (or vertical) direction, the same procedure would yield another  $2 \cdot 2^{L=2} - 3$  independent degenerate configurations (for a grand total of  $4 \cdot 2^{L=2} - 4$ ).

Switching on the interaction  $J$  in Eq. (42) lifts this macroscopic degeneracy by

assigning an energy

$$E_{C_{\text{stagg}}}^{(J)} = E_{C_{\text{stagg}}}^{(J;k)} + E_{C_{\text{stagg}}}^{(J;?) } \quad (44)$$

to each configuration in this manifold. The energy  $E_c^{(J)}$  has been decomposed into two contributions. The first one,

$$\begin{aligned} E_{C_{\text{stagg}}}^{(J;k)} &= \frac{3}{2} J L \quad (L=2) \\ &= \frac{3}{2} \sum_{i=1}^{K=2} J L \end{aligned} \quad (45)$$

does not lift the degeneracy of this manifold and can be thought of as resulting from the zero-point energy of a diagonal labeled by the integer  $i = 1; \dots; L=2$ . The second one,

$$\begin{aligned} E_{C_{\text{stagg}}}^{(J;?) } &= J L \sum_{i=1}^{K=2} \frac{1 + S_i S_{i+1}}{2} + \frac{J L}{2} \quad (L=2) \\ &= \frac{J L}{2} \sum_{i=1}^{K=2} S_i S_{i+1}; \end{aligned} \quad (46)$$

can be thought of as resulting from an Ising interaction between consecutive diagonals whereby the Ising spin  $S_i$  variable takes the value  $+1$  ( $-1$ ) if the diagonal intersects vertical (horizontal) dimers. We have thus mapped the problem of evaluating the energy (42) for all configurations obtained from the seed configuration in Fig. 9(a) by flipping rigidly all the dimers that intersect top-right to bottom-left diagonals as in Fig. 9(a) into an effective one-dimensional Ising model with the extensive exchange energy  $JL=2$ . Observe that the fact that the nearest-neighbor Ising interaction is proportional to the system size in the 1D Ising model (46) implies that (a) the system orders for any non-vanishing value of the dimensionless ratio  $J=T$  and (b) excitations are separated from the ordered state by an energy gap that grows linearly with  $L$ . The Ising order is ferromagnetic when  $J > 0$  and antiferromagnetic when  $J < 0$ . The dimers are all aligned along the same direction when  $J=T > 0$  (parallel staggered order). When  $J=T < 0$ , the dimers are aligned along the same direction within a diagonal but are rotated by  $\pi/2$  between any two consecutive diagonals (alternating staggered order). Equivalent results are obtained if we consider top-left to bottom-right diagonals or a translated starting onfiguration, as discussed above. Therefore, the ground state manifold of energy (42) is four-fold degenerate for any finite  $J$ .

Next, we consider the case of  $u=T=1$  and  $J=T=0$  when the system lies deep in the columnar phase. There are four degenerate columnar ground states one of which is depicted in the left panel of Fig. 9(b) and the other three are obtained upon rotating globally all the dimers by  $\pi/2$  or upon a global translation by one lattice spacing. This degeneracy is preserved when switching on the interaction  $J$ , which

results in the energy

$$E_{\text{Ccol}}^{(J)} = \frac{JL^2}{2} E_{\text{Cstagg}}^{(J)}; \quad (\text{for } J > 0); \quad (47)$$

The equality holds only for the four staggered configurations with alternating dimer directions along any two consecutive diagonals.

Third, we want to estimate the average energy  $E_{\text{dis}}^{(J)}$  of configurations in the disordered phase due to the coupling  $J$ . This is given by

$$E_{\text{dis}}^{(J)} = \frac{J}{2} (2 C_{\text{nn}} + 2 C_{\text{nnn}}) L^2; \quad (48)$$

where  $C_{\text{nn}}$  is the probability to find a pair of parallel nearest-neighbor dimers and  $C_{\text{nnn}}$  is the probability to find a pair of parallel next-nearest-neighbor dimers in the disordered phase. In the non-interacting limit  $u; J \rightarrow 0$ , the probabilities  $C_{\text{nn}}$  and  $C_{\text{nnn}}$  can be obtained exactly in the thermodynamic limit, as illustrated by M. E. Fisher and J. Stephenson in Ref. [4]

$$C_{\text{nn}} = \frac{1}{8}; \quad C_{\text{nnn}} = \frac{1}{4} \frac{1}{2} \frac{1}{2} : \quad (49)$$

Consequently, to leading order in  $L$ , one obtains

$$E_{\text{dis}}^{(J)} = J \left[ \frac{2L^2}{8} + \frac{4L^2}{4} \frac{1}{2} \frac{1}{2} \right] = \frac{JL^2}{2} \frac{(3+4)}{2} \quad (50)$$

in the limit  $u; J \rightarrow 0$ . Notice that if  $J > 0$  then  $E_{\text{dis}}^{(J)} > E_{\text{Ccol}}^{(J)} = E_{\text{Cstagg}}^{(J)}$ . For finite values of the couplings  $J$  and  $u$ , the probabilities  $C_{\text{nn}}$  and  $C_{\text{nnn}}$  in the disordered phase are modified and the above result no longer holds exactly. However, we conjecture that the inequality  $E_{\text{dis}}^{(J)} > E_{\text{Cstagg}}^{(J)}$  holds true throughout the line of critical points separating the columnar phase from the staggered phase for  $J > 0$ . This conjecture is indeed confirmed by our numerical transfer matrix results (e.g., see Fig. 10) that clearly indicate a shrinking of the disordered phase for positive values of  $J$ .

For sufficiently large values of  $J=T$ , the disordered phase is expected to disappear as  $J$  favors the parallel alignment of nearest-neighbor and next-nearest-neighbor dimers. The transition between the staggered and columnar phases is then controlled by the competition between the dimensionless free energies of the two ordered phases

$$\begin{aligned} F_{\text{col}}(T) &= \frac{uL^2}{2T} - \frac{JL^2}{2T} \ln(4); \\ F_{\text{stagg}}(T) &= \frac{JL^2}{T} \ln(4); \end{aligned} \quad (51)$$

where for the staggered case we used the energy and entropy consistent with the

$J > 0$  case. This yields an estimate for the transition to occur when  $J = u$  that is in remarkably good agreement with the numerical results.

Let us now turn to the TM calculations. When  $J > 0$ , the  $W_x = 0$  sector captures the physics of the global transfer matrix much like in the  $J = 0$  case and we can thus use the same type of approach. The critical nature of the disordered phase appears to be preserved by the  $J$  coupling, although its width is gradually reduced in agreement with our conjectured phase diagram in Fig. 8. For brevity, we show in Fig. 10 only the central charge and scaling exponents obtained for  $J=T = 0.5$ . The

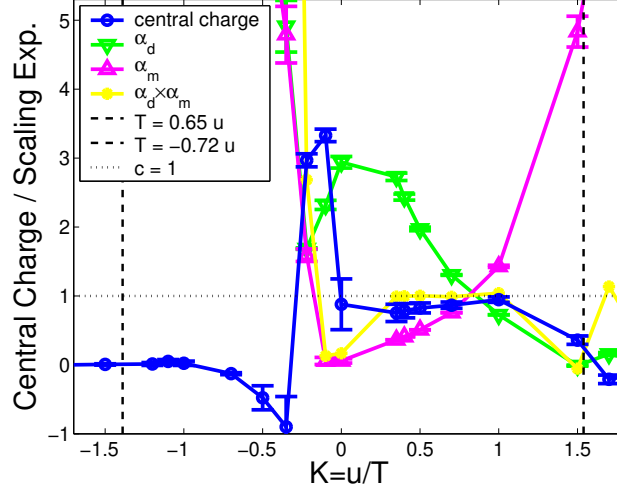


Fig. 10. Central charge and scaling exponents for the electric and magnetic monopole operators as a function of  $K = u/T$ . Positive values of  $K$  correspond to the columnar side of the interaction, while negative ones correspond to the staggered side. Following the convention in Ref. [10], we plot the scaling exponents  $\alpha_d = 2d_{1,0}$  and  $\alpha_m = 2d_{0,1}$  (equal to  $1-g$  and  $g$  from Eq. (22), respectively), instead of the scaling dimensions  $d_{e,m}$ . The value of the reduced coupling constant  $J=T = 0.5$  is held constant throughout. The dashed lines indicate the location of the staggered and columnar transitions in the  $J = 0$  case discussed in Sec. 3.3.

origin of the peak in the central charge appearing at the first order transition to the staggered phase is as of now unclear, though it is likely due to some spurious finite size effect (see also the discussion below on the first order transition between the columnar and staggered phase at low temperatures). For values of the reduced coupling  $J=T$  larger than  $(J=T)_c \approx 0.6$  the critical region shrinks to the point  $J = u$  at which a direct transition between the staggered and the columnar phase takes place. This is in agreement with the free energy arguments of Eq. (51), suggesting that the transition arising from the collapse of the line of critical points is indeed a first order transition. Observe that the first-order critical point  $J = u$  that appears at low temperatures ( $J=T \approx 0.6$ ) is special from an entropic point of view. Indeed, all the configurations obtained from a columnar one through any combination of the translations illustrated in Fig. 9(b) are degenerate in energy when  $J = u$ . While the number of degenerate lowest-energy configurations is finite in the parallel staggered and columnar phase, it becomes exponential in the linear size of the system

at the  $J = 0$  critical point. Namely, there are  $2^L + 2^M$  degenerate configurations in an  $L \times M$  system, whereby  $2^L$  ( $2^M$ ) correspond to having all the dimers aligned horizontally (vertically). Consequently, at the coexistence point  $J = 0$  the intensive entropy of the system scales with system size as

$$\frac{\ln(e^L + e^M)}{LM} : \quad (52)$$

In turn, this gives a contribution to the dimensionless intensive free energy obtained from TM calculations of the form

$$\lim_{M \rightarrow \infty} \frac{\ln(e^L + e^M)}{LM} = \frac{1}{L} : \quad (53)$$

Equation (53) introduces a  $1/L$  finite-size scaling correction, the signature of which is to give rise to a peak in the central charge at  $J = 0$  (it would actually be infinite if the  $L \rightarrow \infty$  extrapolation could be done exactly) when using the  $1/L^2$  finite size scaling Ansatz for the central charge as in Sec. 3.3. We can thus take advantage of this effect, when fitting the free energy as in Eqs. (39) and (40), to interpret the peak in the free energy when  $J=T \approx 0.6$  as a signature of a first order phase transition. A remnant of the  $1/L$  correction to scaling might also be responsible for the central charge peak at the staggered transition that appears in the numerical results when  $J=T \approx 0.6$  (see Fig. 10).

When  $J < 0$ , the numerical analysis becomes more delicate because the staggered order that the system develops at large, negative values of  $J=T$  has alternating dimer directions between consecutive diagonals [see Fig 9(a)]. Studying this phase demands larger lattices due to the symmetry breaking pattern which allows only values of  $L$  that are multiple of 4 in the notation used in Fig. 2. Moreover, this type of order lies in the  $W_x = L/4$  sector and the transition cannot be captured by considering the  $W_x = 0$  sector alone (which is the correct one for the columnar transition). In Fig. 11 we present the results obtained from the  $L = 8;12;16$  data with the global TM. The small number of accessible system sizes does not allow for an appropriate  $L \rightarrow \infty$  extrapolation (40) and the values in Fig. 11 are directly obtained from the finite size scaling fits (39). As expected, upon changing the sign of the coupling  $J$  the disordered phase is now favored over the two ordered ones and the line of critical points appears to expand with respect to the  $J = 0$  case in Fig. 11 (Top). From the behavior of the global and restricted free energies one sees that the correct asymptotic behavior (47)  $\lim_{L \rightarrow \infty} (f) = J=2 = 0.1$  is captured only by the global TM.

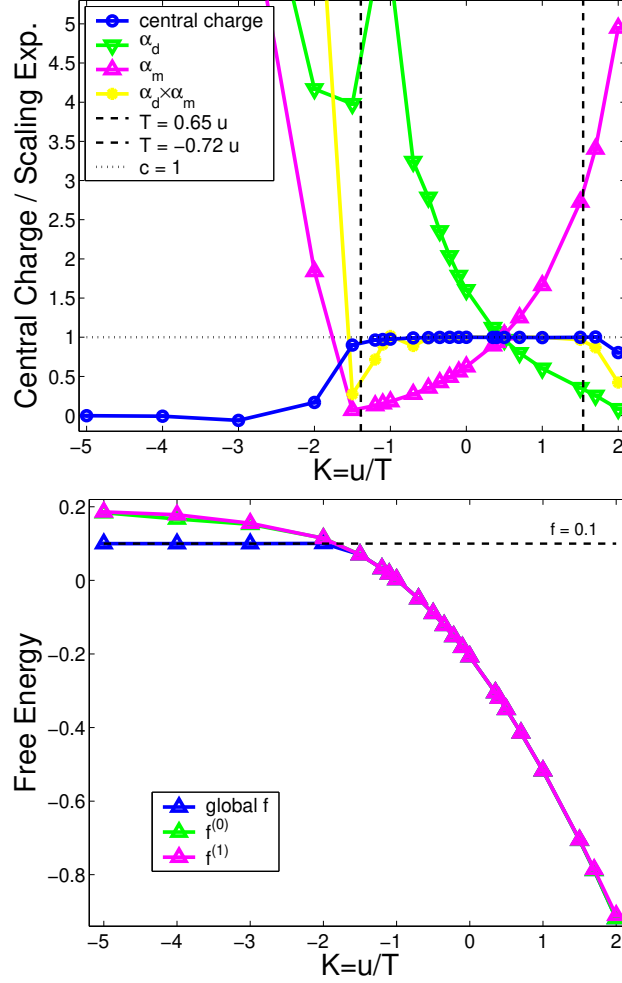


Fig. 11. (Top) Central charge and scaling exponents for the electric and magnetic monopole operators as a function of  $K = u/T$ . Positive values of  $K$  correspond to the columnar side of the interaction, while negative ones correspond to the staggered side. Following the convention in Ref. [10], we plot the scaling exponents  $\alpha_d = 2d_{1,0}$  and  $\alpha_m = 2d_{0,1}$  (equal to  $1-g$  and  $g$  from Eq. (22), respectively), instead of the scaling dimensions  $d_{e,m}$ . The value of the reduced coupling constant  $J=T = 0.2$  is held constant throughout. The dashed lines indicate the location of the staggered and columnar transitions in the  $J = 0$  case discussed in Sec. 3.3. (Bottom) Free energy of the system obtained from the global TM and from the TM restricted to the  $w_x = 0$  and  $w_x = 1$  sectors respectively. Notice that only the global free energy saturates at  $J=2 = 0.1$  for large negative values of  $u=T$ , as expected from Eq.(47).

## 5 The role of defects

The purpose of this section is to generalize Hamiltonian (13) in such a way that the dynamics of defects becomes possible without spoiling the existence of a GS of the form (16). We shall only be concerned with point defects that we call monomers. A monomer is a site of the square lattice that is not the end point of a dimer.

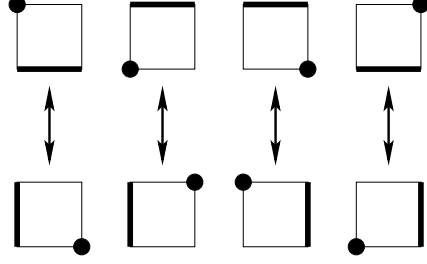


Fig. 12. There are eight ways for a plaquette of the square lattice to accommodate a single monomer (a site occupied by a filled circle) and a single dimer on any of its two remaining free edges. These eight configurations are grouped into pairs that define the local moves in configuration space. Any of these local moves amounts to a rotation by  $\pi/2$  of the dimer and a diagonal hop of the monomer.

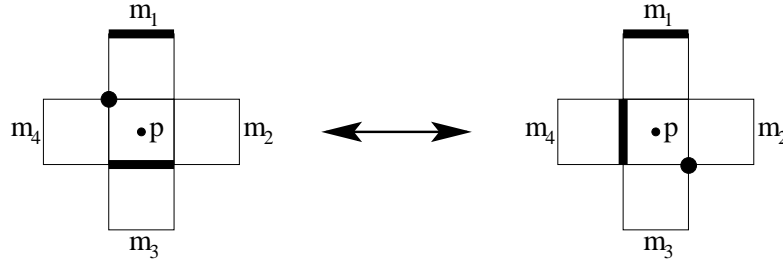


Fig. 13. One of the two pairs of decorated plaquettes  $\gamma_1$  and  $\bar{\gamma}_1$  that involve hopping of the monomer between the upper left and lower right corners of the plaquette  $p$ .

The strategy that we will follow consists of three steps. First, we define the enlarged classical configuration space  $S$  describing a *dilute* SLDM where each site belongs to *at most* one dimer. Second, we define the classical configuration energy

$$E_c^{(u; \cdot)} := u N_c^{(f)} + M_c \quad (54)$$

where  $N_c^{(f)}$  is, as before, the total number of plaquettes occupied by two parallel dimers in configuration  $C$  while  $M_c$  is the total number of monomers in configuration  $C$ . The energy scale  $2/R$  thus plays the role of a chemical potential for the monomers. Third, we need to generalize the local moves  $\gamma_0$  &  $\bar{\gamma}_0$  in the classical configuration space  $S_0$  that we encountered in Fig. 1 to endow monomers with quantum dynamics. To this end, we first define *decorated* plaquettes that involve monomers. Any plaquette of the square lattice has four ways to accommodate a single monomer. Given a plaquette occupied by a single monomer, there are two ways to accommodate a dimer on one of its two remaining free edges. Any plaquette of the square lattice has thus eight ways to accommodate a single monomer and a single dimer. In turn, these eight ways can be grouped into pairs each of which defines a local move in the classical configuration space as shown in Fig. 12. A decorated plaquette  $\gamma_1$  at  $p$  built around a single monomer and a single dimer is obtained by taking Fig. 1 and replacing the flippable plaquette  $p$  by any of the plaquettes in Fig. 12 as is done in Fig. 13. Then, we want to account for the creation and annihilation of pairs of monomers. Following the same steps as above, we in-

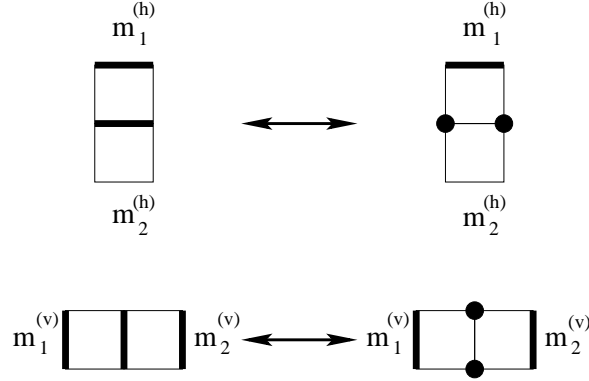


Fig. 14. A pair of decorated horizontal bonds  $\mathbf{b}_2^{(h)}$  and  $\overline{\mathbf{b}_2^{(h)}}$  and a pair of decorated vertical bonds  $\mathbf{b}_2^{(v)}$  and  $\overline{\mathbf{b}_2^{(v)}}$  that are related by the process of creation / annihilation of a pair of monomers. The information encoded by the decorated bond is the location of the bond, whether it is occupied by a dimer or two monomers, and whether the two bonds facing it are occupied by a dimer ( $m_{1;2}^{(h,v)} = 1$ ) or not ( $m_{1;2}^{(h,v)} = 0$ ).

introduce the decorated horizontal and vertical bonds  $\mathbf{b}_2^{(h)}$  and  $\overline{\mathbf{b}_2^{(h)}}$ , as well as the corresponding local updates  $\mathbf{b}_2^{(h)} \S \overline{\mathbf{b}_2^{(h)}}$  and  $\mathbf{b}_2^{(v)} \S \overline{\mathbf{b}_2^{(v)}}$  defined in Fig. 14. For notational simplicity we will omit in the sequel the reference to the bond orientation  $h;v$ , as we have already done for the bond  $b$  and plaquette  $p$  position labels, and for the eight different types of decorated monomer-dimer plaquettes.

The new quantum Hamiltonian can then be assembled from three separate parts, the pure dimer contribution  $\mathbb{H}_0$  and two terms arising from the introduction of monomers,  $\mathbb{H}_1$  and  $\mathbb{H}_2$ ,

$$\begin{aligned}
 \mathbb{H}_{\text{tot}} &= \mathbb{H}_0 + \mathbb{H}_1 + \mathbb{H}_2 \\
 &= \frac{t_0}{2} \sum_{\mathbf{b}_0} e^{u N_{\mathbf{b}_0}^{(f)} = 2T} j_0^{(h)} i h_0^{(h)} j + e^{u N_{\mathbf{b}_0}^{(f)} = 2T} \overline{j_0^{(h)} i h_0^{(h)} j} \quad \overline{j_0^{(h)} i h_0^{(h)} j} + j_0^{(h)} i h_0^{(h)} j \\
 &\quad + \frac{t_1}{2} \sum_{\mathbf{b}_1} e^{u N_{\mathbf{b}_1}^{(f)} = 2T} j_1^{(h)} i h_1^{(h)} j + e^{u N_{\mathbf{b}_1}^{(f)} = 2T} \overline{j_1^{(h)} i h_1^{(h)} j} \quad \overline{j_1^{(h)} i h_1^{(h)} j} + j_1^{(h)} i h_1^{(h)} j \\
 &\quad + \frac{t_2}{2} \sum_{\mathbf{b}_2} e^{(u N_{\mathbf{b}_2}^{(f)} + M_{\mathbf{b}_2}) = 2T} j_2^{(h)} i h_2^{(h)} j + e^{(u N_{\mathbf{b}_2}^{(f)} + M_{\mathbf{b}_2}) = 2T} \overline{j_2^{(h)} i h_2^{(h)} j} \quad \overline{j_2^{(h)} i h_2^{(h)} j} + j_2^{(h)} i h_2^{(h)} j
 \end{aligned} \tag{55}$$

The energy scales  $t_0$ ,  $t_1$ , and  $t_2$  are positive. For any  $n \geq 0; 1g$ , the integer  $N_{\mathbf{b}_n}^{(f)} = N_{\mathbf{b}_n}^{(f)}$  is nothing but the change  $N_{\mathbf{b}_n}^{(f)} - N_{\mathbf{b}_n}^{(f)}$  in the number of flippable plaquettes induced by the local update  $\mathbf{b}_n \S \overline{\mathbf{b}_n}$  when the action of  $j_n^{(h)} i h_n^{(h)} j$  on the state  $\mathfrak{C}_i$  is non-vanishing (or, equivalently, when the action of  $\overline{j_n^{(h)} i h_n^{(h)} j}$  on the updated state



$\bar{\mathcal{C}}_i$  is non-vanishing). The integer  $M_{\frac{1}{2}} = \frac{M-1}{2}$  takes the value  $+2$  when two monomers are created and the value  $-2$  when two monomers are annihilated under the local update  $\frac{1}{2} \rightarrow \frac{1}{2}$ . We leave it as an exercise to the reader to express  $N_{\frac{1}{2}}^{(f)}$  in terms of the integers  $m_{1,2,3,4}$  defined in Fig. 13 and in terms of the integers  $m_{1,2}^{(h,v)}$  defined in Fig. 14.

As desired, the GS of Hamiltonian (55) is given by

$$|j\rangle_{\text{tot}} = \sum_{C2S} e^{(uN_c^{(f)} + M_c)/2T} \bar{\mathcal{C}}_i \quad (56)$$

where the summation has been extended to account for the enlarged Hilbert space. By construction monomers always occur in pairs with one half of the monomers residing on one of the sublattice of the square lattice. The zero-temperature phase diagram of the quantum Hamiltonian (55) thus contains the finite- $T$  phase diagram of the classical system with the partition function

$$Z(T=u; \beta=T) = \sum_{C2S} \exp \left[ -\frac{E_c^{(u; \beta)}}{T} \right] = \sum_{C2S} \exp \left[ -\frac{uN_c^{(f)} + M_c}{T} \right] : \quad (57)$$

A detailed study of the phase diagram of this partition function is beyond the scope of the present paper. However, according to some preliminary results by Alet *et al.* in Ref. [10], we anticipate a rich and interesting structure, qualitatively illustrated in Fig. 15. Notice that the  $u = 0, \beta = 1$  limit realizes precisely the RK point (2). Also, although the effect of a finite concentration of static monomers on the classical critical phase is an interesting open problem, one can reasonably expect that the spatial dimer correlations will be preserved below a cutoff length scale dictated by the average monomer-monomer separation. Therefore, the limit  $t_2 = 0$  realizes a classical neutral gas of charged hard-core particles (the monomers) at a fixed density, coupled to a *quasi-critical* environment (the dimers).

Finally, having constructed a quantum dilute SLDM Hamiltonian using the Stochastic Matrix Form decomposition (55) offers the advantage of obtaining (static) GS correlation functions directly from the associated classical system, as pointed out in Sec. 1. The possibility to use classical numerical techniques, such as Monte Carlo simulations and transfer matrix calculations, in the *same number of dimensions* gives access to much larger system sizes than quantum techniques, such as quantum Monte Carlo or exact diagonalization routines, do. These classical results allow to contrast quantum dynamical correlation functions of monomers against static correlation functions inherited from the classical partition function (57). In this context, related quantum dimer models with mobile holes have been studied by exact-diagonalization, Green-function, and classical Monte Carlo techniques by Poilblanc and collaborators [58].

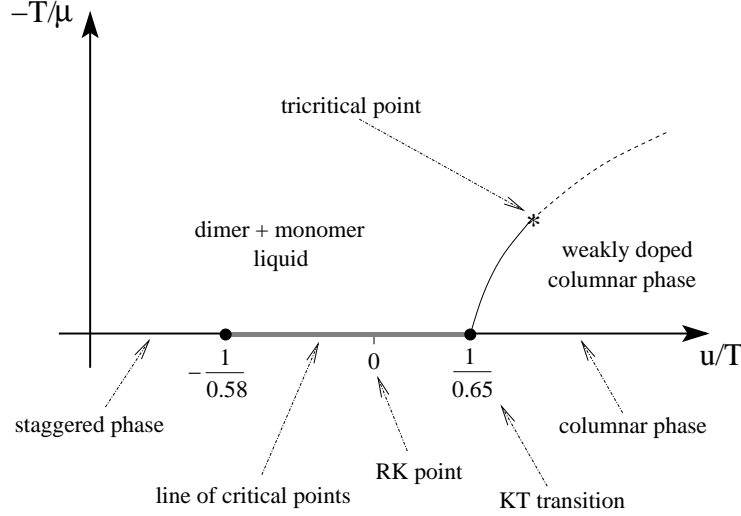


Fig. 15. Conjectured phase diagram of the classical partition function (57) after Alet *et al.* in Ref. [10] that is inherited by the SMF quantum dimer model (56). While for  $u=T < u=T_c^{(\text{columnar})}$  the introduction of monomers is a relevant perturbation – which destroys the critical phase – it becomes marginal at  $T_c^{(\text{columnar})}$ . Therefore, a phase boundary  $(T)$  is expected to depart from the KT transition point at  $(T; u) = (T_c^{(\text{columnar})}; 1)$ . In the close vicinity of  $(T; u) = (T_c^{(\text{columnar})}; 1)$ , this phase boundary separates a weakly doped columnar ordered phase from a dilute (non-critical) dimer liquid and the transition between these two phases is expected to be continuous (solid line at the phase boundary). For both  $T =$  and  $u=T$  large, the phase boundary  $(T)$  separates phases of matter with large gaps and the transition between these two phases is expected to become first order (dashed line at the phase boundary). A *tricritical point* at some finite  $(T; u)$  must then separate the first order from the continuous behavior along the phase boundary. Alet *et al.* give an estimate for the tricritical point at  $T = u = 0.39(4)$  and  $u = 0.25(10)$  [10].

### 5.1 The non-interacting monomer gas in a critical background

In closing, we would like to discuss briefly a special case of the Hamiltonian in Eq. (55), namely the one we obtain upon choosing  $t_0 = t_1 = 0$  and  $u = 0$ . Given this choice,  $t_2$  becomes just a scale factor and can be conveniently set to 1. Also, the information about the integers  $m_{1,2}^{(h,v)}$  defined in Fig. 14 is no longer needed and can be dropped. The new Hamiltonian thus obtained can be written in a symbolic notation along the line of Eq. (1) as

$$\mathcal{H}_{\text{mon}} = \sum_b e^{-T} \sum_i j_{i,i+h}^x j_{i,i+h}^y + e^{-T} \sum_i j_{i,i+h}^x j_{i,i+h}^y + j_{i,i+h}^x j_{i,i+h}^y + j_{i,i+h}^x j_{i,i+h}^y ; \quad (58)$$

where the summation is over all vertical and horizontal bonds  $b$  and the Hilbert space is the same as for Eq. (55). The exact GS of this Hamiltonian

$$|j_{\text{mon}}\rangle = \sum_{C \in \mathcal{S}} e^{M_C = 2T} \mathcal{F}_C |j\rangle \quad (59)$$

is then captured by the classical dilute dimer model in the sole presence of a chemical potential  $\mu$  for the monomers,

$$Z_{\text{mon}} = \sum_{\{c, s\}} e^{\beta \mu c} : \quad (60)$$

In the limit of  $\beta \mu \rightarrow 1$ , the monomers behave like deconfined virtual particles in a critically correlated dimer background, and the GS wavefunction becomes exponentially close to the GS wavefunction of the RK Hamiltonian (1) at the so called RK point (3).

## 6 Conclusions

In this paper, we constructed an interacting quantum dimer model with a Hamiltonian obeying a Stochastic Matrix Form decomposition [33]. This allowed us to define an associated classical system whose thermodynamic equilibrium correlation functions reflect the behavior of some equal-time ground state expectation values. Using this correspondence, we showed that the quantum system exhibits a line of quantum critical points that separates two ordered GS of the valence bond crystal type. One end point of this line of critical points corresponds to KT transition in the associated classical system. The other one is a first order phase transition. The locality of our SMF quantum Hamiltonian can be used to argue that the dynamical exponent  $z$  is finite, and likely to be  $z = 2$ , along the line of critical points. If so, one can deduce the power-law decay of quantum correlations in time from the behavior of the equal-time spatial correlations. In this sense, the quantum system inherits a KT transition from its associated classical system.

We also studied the robustness of this line of critical points to the introduction of longer-range – yet finite – dimer-dimer interactions. In particular we showed how, for some choice of the additional interaction, one can tune the width of the line of critical points until it gradually collapses onto a single, tricritical point, where the KT and first-order transition meet.

Eventually, we included monomers in the quantum system, i.e., we allowed for sites that are not occupied by a dimer. In doing so, we preserved the SMF structure of the Hamiltonian, thus being able to study the GS properties of the quantum system via an associated classical dilute dimer model. Using this correspondence, we derived qualitatively the zero-temperature phase diagram of the quantum dilute dimer model, opening the possibility to obtain equal-time monomer correlation functions from classical numerical techniques. While this allows access to much larger system sizes to study zero-temperature spatial correlation functions, unequal-time monomer correlations remain the prerogative of quantum MC or exact diagonalization studies.

P.P. would like to thank Didier Poilblanc and Fabien Alet for early discussions and sharing their results prior to publication. C.C. would like to thank Cristian D. Batista for explaining useful details of Ref. [57]. We would also like to thank Eduardo Fradkin for his insightful comments.

## References

- [1] R. H. Fowler and G. S. Rushbrooke, Trans. Faraday Soc. **33** (1937) 1272.
- [2] W. Thurston, Am. Math. Monthly **97** (1990) 757; Richard Kenyon, math-ph/0405052.
- [3] P. W. Kasteleyn, Physica (Amsterdam) **27** (1961) 1209 and J. Math. Phys. **4** (1963) 287.
- [4] M. E. Fisher, Phys. Rev. **124** (1961) 1664, J. Math. Phys. **4** (1963) 278, and J. Math. Phys. **7** (1966) 1776; M. E. Fisher and J. Stephenson, Phys. Rev. **132** (1963) 1411.
- [5] J. Kondev and C. L. Henley, Phys. Rev. B **52** (1995) 6628.
- [6] J. Kondev and C. L. Henley, Nucl. Phys. B **464** (1996) 540.
- [7] P. Fendley, R. Moessner, and S. L. Sondhi, Phys. Rev. B **66** (2002) 214513.
- [8] W. Krauth and R. Moessner, Phys. Rev. B **67** (2003) 064503.
- [9] D. A. Huse, W. Krauth, R. Moessner, and S. L. Sondhi, Phys. Rev. Lett. **91** (2003) 167004.
- [10] F. Alet, J. L. Jacobsen, G. Misguich, V. Pasquier, F. Mila, and M. Troyer, Phys. Rev. Lett. **94** (2005) 235702.
- [11] S. A. Kivelson, D. S. Rokhsar, and J. P. Sethna, Phys. Rev. B **35** (1987) 8865.
- [12] D. S. Rokhsar and S. A. Kivelson, Phys. Rev. Lett. **61** (1988) 2376.
- [13] L. S. Levitov, Phys. Rev. Lett. **64** (1990) 92.
- [14] E. Fradkin, *Field Theories of Condensed Matter Systems*, Addison-Wesley, Redwood City, 1991, Chapter 6.
- [15] P. W. Leung, K. C. Chiu, and K. J. Runge, Phys. Rev. B **54** (1996) 12938.
- [16] C. L. Henley, J. Stat. Phys. **89** (1997) 483.
- [17] R. Moessner and S. L. Sondhi, Phys. Rev. Lett. **86** (2001) 1881.
- [18] R. Moessner, S. L. Sondhi, and P. Chandra, Phys. Rev. B **64** (2001) 144416.
- [19] R. Moessner, S. L. Sondhi, and E. Fradkin, Phys. Rev. B **65** (2002) 024504.
- [20] A. Ioselevich, D. A. Ivanov, and M. V. Feigelman, Phys. Rev. B **66** (2002) 174405.
- [21] G. Misguich, D. Serban, and V. Pasquier, Phys. Rev. Lett. **89** (2002) 137202, and Phys. Rev. B **67** (2003) 214413.
- [22] R. Moessner and S. L. Sondhi, Phys. Rev. B **68** (2003) 054405.
- [23] R. Moessner and S. L. Sondhi, Phys. Rev. B **68** (2003) 184512.
- [24] M. Freedman, C. Nayak, and K. Shtengel, cond-mat/0309120.
- [25] M. Hermele, M. P. A. Fisher, and L. Balents, Phys. Rev. B **69** (2004) 064404.
- [26] E. Fradkin, D. A. Huse, R. Moessner, V. Oganesyan, and S. L. Sondhi, Phys. Rev. B **69** (2004) 224415.

- [27] G. Misguich, D. Serban, and V. Pasquier, J. Phys.: Cond. Mat. **16** (2004) S823.
- [28] C. L. Henley, J. Phys. C **16** (2004) S891.
- [29] E. Ardonne, P. Fendley, and E. Fradkin, Annals of Physics (N.Y.) **310** (2004) 493.
- [30] D. A. Ivanov, Phys. Rev. B **70** (2004) 094430.
- [31] Gregoire Misguich, Vincent Pasquier, Frederic Mila, and Claire Lhuillier, Phys. Rev. B **71** (2005) 184424.
- [32] Arnaud Ralko, Michel Ferrero, Federico Becca, Dmitri Ivanov, and Frederic Mila, Phys. Rev. B **71** (2005) 224109.
- [33] C. Castelnovo, C. Chamon, C. Mudry, and P. Pujol, Ann. of Phys. (N.Y.) **318** (2005) 316.
- [34] K. S. Raman, R. Moessner, and S. L. Sondhi, Phys. Rev. B **72** (2005) 064413.
- [35] M. Freedman, C. Nayak, and K. Shtengel, Phys. Rev. Lett. **94** (2005) 066401.
- [36] O. F. Syljuåsen, Phys. Rev. B **71** (2005) 020401(R), Int. Jour. Mod. Phys. B **19** (2005) 1973, and preprint: cond-mat/0512579.
- [37] A. W. Sandvik and R. Moessner, preprint: cond-mat/0507277.
- [38] R. Moessner, K. S. Raman, and S. L. Sondhi, preprint: cond-mat/0510498.
- [39] Doron L. Bergman, Gregory A. Fiete, and Leon Balents, Phys. Rev. Lett. **96** (2006) 097207 and preprint: cond-mat/0511176.
- [40] T. Senthil, Leon Balents, Subir Sachdev, Ashvin Vishwanath, and Matthew P. A. Fisher, Phys. Rev. B **70** (2004) 144407.
- [41] Leon Balents, Lorenz Bartosch, Anton Burkov, Subir Sachdev, and K. Sengupta, Phys. Rev. B **71** (2005) 144508 and (2005) 144509.
- [42] S. Chakravarty, Phys. Rev. B **66** (2002) 224505.
- [43] C. Castelnovo, C. Chamon, C. Mudry, and P. Pujol, Phys. Rev. B **73** (2006) 144411 and preprint: cond-mat/0512258.
- [44] John A. Hertz, Phys. Rev. B **14** (1976) 1165.
- [45] M. B. Hastings, Phys. Rev. B **69** (2004) 104431.
- [46] M. Freedman, C. Nayak, and K. Shtengel, Phys. Rev. Lett. **94** (2005) 147205.
- [47] G. Grinstein, Phys. Rev. B **23** (1981) 4615.
- [48] Pouyan Ghaemi, Ashvin Vishwanath, and T. Senthil, Phys. Rev. B **72** (2005) 024420.
- [49] K. Shtengel, C. Nayak, W. Bishara, and C. Chamon, J. Phys. A: Math. Gen. **38** (2005) L589.
- [50] Stefanos Papanikolaou, Erik Luijten, and Eduardo Fradkin, abstract N45.00012, APS March meeting 2006, (in preparation).
- [51] <http://www.caam.rice.edu/software/ARPACK/>.
- [52] J. L. Jacobsen and J. Kondev, Nucl. Phys. B **532** (1998) 635; and references therein.
- [53] The reasons for this choice of values of  $L$  is similar to the one discussed in Sec. 4.1. Namely, using the global TM and the full range of values of  $L = 6; 8; 10; 12; 14; 16$  we noticed an oscillatory behavior of the estimants for the central charge  $c(L_0; L_{\max})$  and scaling dimensions  $d_{\text{epm}}(L_0; L_{\max})$  as a function of  $L_0$  (see Sec. 3.3). This usually signals the presence in the system of fluctuations with a spatial periodicity larger than the one generically

allowed by  $L$  (two lattice spacings). Choosing  $L$  to be a multiple of 4 seems to be sufficient in our case to get rid of this spurious behavior.

- [54] C. Castelnovo, P. Pujol, and C. Chamon, Phys. Rev. B **69** (2004) 104529.
- [55] E. N. M. Cirillo, G. Gonnella, and A. Pelizzola, Phys. Rev. E **53** (1996) 1479.
- [56] Notice however that the two ordered phases separated by the tricritical point may differ from those in the RK Hamiltonian, if the presence of a resonating valence bond phase was to be confirmed in the latter model.
- [57] C. D. Batista and S. A. Trugman, Phys. Rev. Lett. **93** (2004) 217202.
- [58] D. Poilblanc, F. Alet, F. Becca, A. Ralko, F. Trouselet and F. Mila, submitted to Phys. Rev. B (RC) and preprint: cond-mat/0602256 .